ENHANCED TISSUE ENGINEERING PROPERTIES OF OSTEOINDUCTIVE CHITOSAN HYDROGEL

A Thesis

presented to

the Faculty of the Graduate School

at the University of Missouri-Columbia

In Partial Fulfillment

of the Requirements for the Degree

Master of Science

---

by

BLAKE THOMAS DARKOW

Dr. Bret Ulery, Thesis Supervisor

MAY 2022

The undersigned, appointed by the dean of the Graduate School, have examined the thesis entitled

ENHANCED TISSUE ENGINEERING PROPERTIES OF OSTEOINDUCTIVE CHITOSAN HYDROGEL

presented by Blake Darkow, a candidate for the degree of Master of Science, and hereby certify that, in their opinion, it is worthy of acceptance.

_____

Professor Bret Ulery

_____

Professor Ciaxia Wan

_____

Professor D Cornelison

ACKNOWDLEGEMENTS

There is no shortage of people to whom I am incredibly greatful to for their help and support throughout my time as a graduate student at the University of Missouri. First off, I would like to thank my research advisor, Professor Bret Ulery, for his constant encrouagement and guidance he has so genoursly given me over the past three and a half years. He cultivates an environment that bolsters us students personally, professionally, and academically. His dedication to his students while challenging them should not go unrecognized. Additonally, I would like to thank the other members of my thesis committee, Professors Ciaxia Wan and D Cornelison, for their support and willingness to serve in this way.

Additionally, I want to thank my fellow researchers without whom I could not have completed this research. Specifically, I had the privelidge to work with a number of undergraduates who contributed significantly to this project including Ellie Snoke, Abigail Grisolano, Megan Mozingo, and Chavis Furgeson. Yisheng Sun, a member of Professor Wan's research group, has been incredibly helpful with all of his knolwdge and work completed on the cellulose side of this research. Finally, I'd like to acknowledge all of the other members of the Biomodulatory Materials Engineering Laboratory (BioMEL). Because of them, I have been continuously encouraged and pushed to complete this venture.

Table of Contents

List of Figures

List of Tables

Abstract

Lower back pain is a considerable medical problem that will impact 80% of the U.S. population at some point in their life. With the most severe cases, surgical repair is necessary and is associated with costs upwards of $10.2 billion annually in the United States. To allieviate back pain, spine fusions are a common treatment in which two or more vertebrae are biologically fused together often through the use of a graft material. Unfortunately, iliac crest bone autograft, the current gold standard graft material, can yield insufficient fusion and is associated with considerable donor site morbidity and pain as well as limited supply. Therefore, new materials need to be developed in order to better coordinate healing and new bone growth in the affected area to reduce unnecessary patient burden. In order to address this issue, the incorporation of allograft and one of two types of cellulose (*i.e.*, ^{0}CNCs and CNFs) into a dual-crosslinked chitosan hydrogel loaded with bioactive calcium phosphate was investigated. Hydrogels were then tested for both their material and biological properties. Specifically, hydrogel swelling ratio, mass loss, ion release profile, compressive strength, biocompatibility, and osteoinduction were determined. Cellulose and allograft incorporation significantly improved compressive strength and biocompatibility. CNFs were found to be a significantly more biocompatible form of cellulose when compared to ^{0}CNCs. Additionally, through the controlled delivery of osteoinductive simple signaling molecules (*i.e.*, calcium and phosphate ions), CNF/Chitosan hydrogels were able to induce osteoblast-like activity in murine mesenchymal stem cells. This research

provides support for our novel material to be further investigated *in vivo* for its application in spine fusion procedures.

Chapter 1. Introduction

Lower back pain is a considerable medical problem impacting 80% of the United States population at some point in their life.[1,2] It is the second most common reason for doctor's visits in the United States and greatest cause of workplace absence in the U.K.[3] While only a minority of the most severe cases require surgery, they account for 29.3% of the total expenditures associated with lower back pain.[4] Reports on the total healthcare spending of these procedures vary widely, from $784 million to $10.2 billion annually in the United States.[4,5] Regardless of which figure is accurate, the burden of lower back pain on society is immense.

Conventional treatment for lower back pain involves an escalation of invasiveness starting with conservative options such as physical therapy before progressing to less-invasive surgeries such as disc repair and replacement. If these approaches do not address a patient's symptoms, then spinal fusion may be necessary.[3] Spinal fusion procedures aim to alleviate back pain brought on by preexisting conditions through mechanically and biologically fixing two or more adjacent vertebrae through the use of instrumentation and/or bone graft materials. The total volume of fusion procedures only continues to rise (from 164,527 in 2004 to 281,575 in 2015) as the U.S. population ages.[5] Despite the significant increase in cases, the rate of fusion achieved clinically varies widely among different bone graft materials from as low as 40% to as high as nearly 100%.[5,6] Additionally, the current gold standard for graft material (*i.e.*, iliac crest bone autograft) is associated with considerable donor site morbidity and pain as well as limited supply.[7] The

significant drawbacks associated with the currently available treatment options as well as increases in the number of procedures performed annually highlights the need for new bone graft substitutes to be developed.

Recent efforts by the biomaterials community have been focused on utilizing tissue engineered scaffolds to mimic the physical, chemical, and biological constructs that exist in natural tissues in order to coordinate healing. Our research groups have focused on the utilization of simple signaling molecules to influence the differentiation of select cell populations to regenerate tissues of interest. For spinal fusion applications, we have developed an osteoinductive biomaterial comprised of a dual-crosslinked, cellulose-supported chitosan hydrogel loaded with bioactive calcium phosphate.[8-10] This hydrogel is designed to release calcium and phosphate ions within a previously defined therapeutic window in order to induce osteoinduction in mesenchymal stem cells. This desirable bioactivity was previously achieved by the dissociation of a phosphate crosslinker[8] and later by controlled release from dibasic calcium phosphate.[9] While this has laid the groundwork for the use of this biomaterial for spinal fusion procedures, there remains significant work to be conducted to continue the development of this hydrogel before it can be motivated to the clinic.

The primary aim of this research is to expand the knowledge surrounding materials for bone tissue engineering applications. Specifically, improvements to the osteoinductive, cellulose-reinforced chitosan hydrogel developed in this lab will be made with focus on its utilization in lumbar fusion procedures to treat lower back pain. Despite significant progress in the development of this material, our

previously published work falls short of reaching the *in vitro* mechanical and biocompatible benchmarks necessary to be studied *in vivo* in appropriate animal models. For example, the compressive strength of the current formulation falls is lower than that of natural bone and the hydrogels have been found to suppress the proliferation of mesenchymal stem cells which are crucial for bone regeneration. Through this research, a solution to the mechanical and biocompatability drawbacks of our first-generation hydrogel has been found.

Chapter 2. Literature Review

2.1 Spine

The spine is an essential structure of the body consisting of stacked vertebrae that allow movement and provide support to the upper regions of the body and protect the spinal column, the neural conduit between the brain and the peripheral nerve system. Due to its complex nature, a variety of diseases and injuries may occur to the spine that require surgical intervention. Of the procedures available, spine fusion remains a commonly performed approach in which two or more adjacent vertebrae are fixed together using instrumentation for stabilization and/or graft materials to facilitate bony fusion. While the instrumentation used in spinal fusion is quite standard, there are many different graft materials that are currently employed, though they all have considerable drawbacks. Therefore, the generation of novel graft materials continues to be an area of considerable research. To understand the use of biomaterials in spine fusion, the complex anatomy and physiology of the vertebrae needs to first be discussed.

2.2 Vertebral Anatomy & Physiology

2.2.1 Bone Modeling and Remodeling

The structural functions of bone and its management of systemic calcium and phosphate levels are achieved by a complex and choreographed balance between the three major bone cell types: osteoblasts, osteoclasts, and osteocytes.[11] Together these cells turnover (*i.e.*, deposit and break down) the extracellular matrix that encapsulates them which is comprised of proteins (*i.e.*, mostly collagen) and ceramic (*i.e.*, primarily hydroxyapatite, HA -

$Ca_{10}(PO_4)_6(OH)_2$). Specifically, osteoblasts, the primary bone building cells, secrete extracellular collagen matrix as well as osteocalcin to promote mineral deposition in a process called osteogenesis or bone deposition.[12] These cells differentiate from mesenchymal stem cells (MSCs) or mesenchymal-derived progenitor cells, through activation of a number of signaling cascades as well as in response to various environmental factors.[13-15] Osteoclasts are differentiated from bone marrow-derived macrophages and counterbalance osteoblast bone formation by breaking down bone matrix in a process called bone modeling or resorption.[15] The third cell type, osteocytes, are osteoblasts that become entrapped in the bone matrix where they regulate bone remodeling via hormonal and mechanical signals.[16] This process shapes bone to fit their physical environment and helps to regulate systemic calcium and phosphate levels.

Bone remodeling not only works to maintain the musculoskeletal support system, but also regulates systemic calcium ion (Ca^{2+}) and phosphate ion (PO_4^{3-}) levels within desirable physiological limits. This regulation is controlled by four hormones: calcitonin, parathyroid hormone (PTH), vitamin D_3, and estrogen. Calcitonin stimulates bone deposition by osteoblasts and directly inhibits bone resorption by osteoclasts leading to lower systemic ion levels.[17] On the other hand, PTH and vitamin D_3 both cause a rise in blood serum Ca^{2+} levels by encouraging osteoclast bone resorption in which HA undergoes decomposition into Ca^{2+} and PO_4^{3-}. Estrogen, which naturally occurs in females and is converted from testosterone in males, promotes bone mineralization by reducing apoptosis in osteoblasts and osteocytes.[18] Additionally, estrogen inhibits bone resorption by signaling

osteoclast apoptosis which, in turn, delays the onset of osteoporosis.[11,19] Hormone-based bone regulation, and its lack thereof in later age, can greatly impact bone density especially in the bones of the spine.

2.2.2 Vertebral Complex Anatomy & Biomechanics

The human spine consists of 33 individual vertebrae and is divided into 5 regions. The 7 vertebrae at the top make up the cervical section in the neck and are labeled C1 - C7. The next 12 vertebrae comprise the thoracic region anchoring the ribs and are identified as T1 - T12. The 5 vertebral bodies of the lumbar region (L1 - L5) are found in the lower back and support the upper regions of the spine. Most of the body's weight and movement is dependent on the structural integrity of the lumbar spine which leads to a high prevalence of injuries and degenerative disease in this region.[20] The sacrum is comprised of five vertebral bodies (S1 - S5) that fuse in the womb and are attach to the medial region of the pelvis. Finally, the coccyx, colloquially known as the tailbone, is made of 4 fused vertebrae that anchor the pelvic floor muscles. Unlike the fused sacrum and coccyx, the cervical, thoracic, and lumbar regions allow mobility and flexion between the bodies due to their irregular shape and location in relation to one another.

Each vertebra in the upper three regions (*i.e.*, cervical, thoracic, and lumbar) share many common features. Their vertebral bodies support the weight of the column above it and form the vertebral canal that protects the spinal cord and its nerve supply to the body.[20] Vertebral bodies increase in size as you go down the spine as they must support the heavier loads of the body above them. Facet joints are cartilaginous points of contact between vertebrae which allow for stability and

translation between levels. Between each vertebral body is an intervertebral disc which acts as a cushion absorbing compressive and torsional stress between the levels. Pedicles attach the lamina on the posterior side of the vertebrae forming the vertebral canal. Transverse and spinal processes are attachment points for many muscles and ligaments and protrude from the lamina laterally and posteriorly, respectively. All of these features form the vertebral column that serves as the body's vertical support structure and protects the spinal cord connecting the brain with the rest of the body.[20]

2.2.3 Disease pathologies of lumbar vertebrae

Of the three non-fused regions of the spine, the lumbar region is the most often injured due to the increased mechanical stress placed on this lower region.[21,22] As a result, a variety of serious medical issues may occur, specifically the three most common disorders – disc degeneration, spondylolisthesis, and stenosis – all of which are indications for surgical intervention like spinal fusion.[5]

2.2.3.1 Degenerative Disc Disease

Degenerative disc disease (DDD) is a chronic condition, which often manifests clinically as neck and back pain and occurs when the intervertebral disc loses its structural integrity.[22] With age, the nucleus of the disc becomes less elastic, more fibrous, and the area becomes inhospitable to the fibroblast cells that are crucial for the regulation and maintenance of the tissue.[23] More than 86% of patients ages 50 and older have some form of lumbar disc degeneration.[22] That being said, some forms of the disease do not result in considerable disability.[5,23]

A common manifestation of DDD is disc herniation which is the displacement of a disc beyond its normal margins within the intervertebral space.[24] Disc herniation is the leading cause of lower back pain affecting 1 to 5% of the population annually.[1,25] Surgical treatment of disc herniation has long been controversial given most cases can be resolved through the use of non-operative approaches.[1,5,25] However, a recent meta-analysis found surgical intervention to be more effective at alleviating symptoms of disc herniation when compared to conservative non-surgical treatment options.[24] Disc herniation specifically accounted for approximately 17.5% of lumbar fusions between the years 2004 and 2015.[5]

2.2.3.3 Spondylolisthesis

Spondylolisthesis consists of anterior displacement of the vertebral body caused by an anatomical defect or fracture of the vertebral arch (*i.e.*, spondylosis). Spondylosis is absent at birth, prevalent in 4.4% of the population by age 6, and is present in 6% of all adults.[26,27] If spondylosis progresses to spondylolisthesis, it may cause compression of the nerve root inducing sharp leg pain.[26] Spondylolisthesis is the most common spinal disorder diagnosis requiring lumbar spine fusion as it was responsible for 45.2% of lumbar spine fusions in 2015.[5]

2.2.3.4 Spinal Stenosis

Lumbar spinal stenosis (LSS) is a condition which arises from the overgrowth of previously injured bone, ligaments, and tissue of the lower spine resulting in compression on the spinal cord and it vasculature in the spinal canal.[28] The condition intensifies with age and was present in 77.9% of individuals over the

age of 40 as identified by radiographic data from the Wakayama Spine Study.[29] However, only 12.2% of those with radiographic LSS presented with any significant clinical symptoms.[29] In 2015, 17.6% of spine fusions in the United States were due to managing LSS.[5] The use of spinal fusion to address this disease, like with disc herniation and spondylolisthesis, is dependent on its severity and the lack of success achieved with more conservative treatment approaches.

2.3 Lumbar Spine Fusion Procedures

Lumbar spine fusion is an accepted surgical intervention that can treat a variety of spinal disorders including, but not limited to, those already mentioned.[5,24,30,31] Primary lumbar spine fusion techniques are defined by the surgical approach utilized and are listed as follows; posterolateral fusion (PLF), anterior lumbar interbody fusion (ALIF), oblique lumbar interbody fusion / anterior to psoas (OLIF/ATP), lateral lumbar interbody fusion (LLIF or XLIF), transforaminal lumbar interbody fusion (TLIF), and posterior lumbar interbody fusion (PLIF).[31] The inclusion of “interbody” in a technique indicates the fusion of adjacent vertebral bodies, generally with a spacer implant made of PEEK or Titanium.[32] A general diagram of the anatomy and implanted materials can be seen in **Figure 1**. Each case may not use all the illustrated instrumentation and materials, and the specific indication can change the required surgical approach significantly.[31]

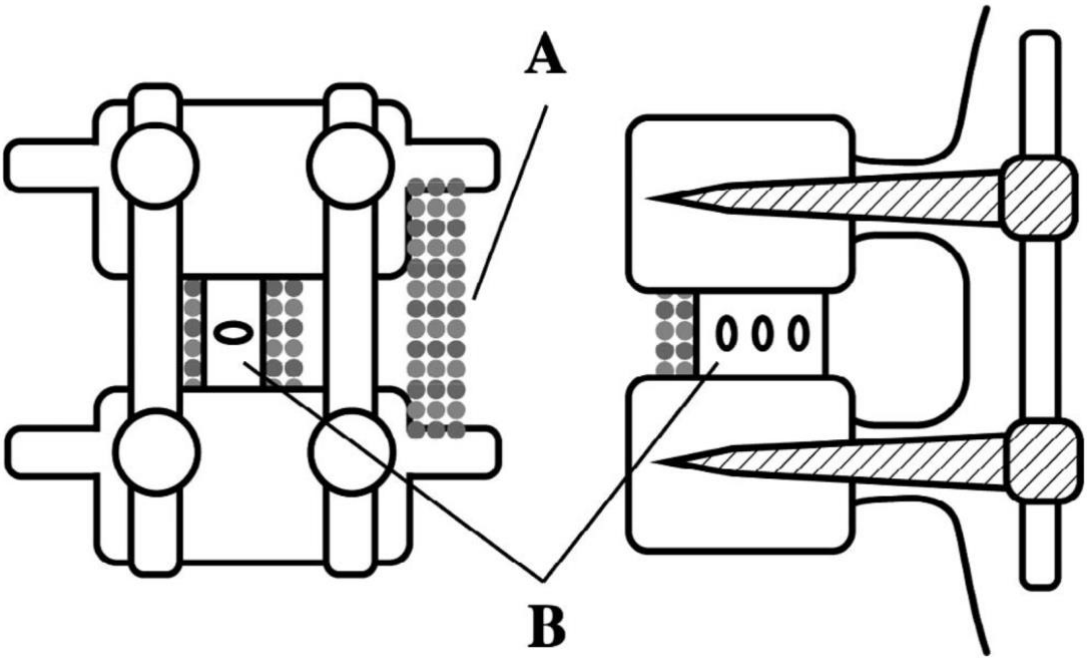

Figure 1. Diagram of single-level spine fusion including instrumentation. **(A)** This location demonstrates a graft material placed between the transverse processes. **(B)** In contrast, this location shows graft material and an intervertebral spacer utilized to induce fusion between the vertebral bodies themselves. Artwork reprinted from previously published work.[33]

2.3.1 Surgical Approaches

2.3.1.1 PLF

Posterolateral fusion was one of the first widely accepted approaches and is performed by making a posterior mid-line incision which provides access to the spinous and transverse processes.[34] Graft material is bridged across the adjacent transverse processes and commonly secured with pedicle instrumentation. A laminectomy may also be performed in order to relieve the pressure being placed on the spinal canal.

2.3.1.2 PLIF

Posterior lumbar interbody fusion was the first lumbar interbody fusion approach developed and is performed via a midline incision to access levels L1 - S1. Using this method, a laminotomy is required to access the interbody space. Despite this access limitation, the PLIF approach provides appropriate interbody height restoration, neural decompression, and easy access to implant posterior instrumentation for support.[35]

2.3.1.3 TLIF

Transforaminal lumbar interbody fusion is performed by making a midline or bilateral paramedian incision which allows access to the interbody space for levels between L1 - S1. This approach allows for the implementation of posterior instrumentation while reducing surgical trauma to the spinal muscles and vertebrae.

2.3.1.4 LLIF/XLIF

The lateral (or extreme) interbody fusion approach is performed by accessing the interbody space by creating a lateral retroperitoneal, transpsoas corridor. This approach allows access to the interbody spaces between T12/L1 and L4/L5, but is limited in reaching the L5/S1 due to the location of the iliac crest. While it provides excellent access for conditions such as sagittal/coronal deformities and degenerative scoliosis with laterolisthesis, it cannot provide access to the central canal nor provide any biomechanical support without the use of posterior instrumentation.[36,37]

2.3.1.5 OLIF/ATP

The oblique lumbar interbody fusion / anterior to psoas approach is made through a lateral and paramedian incision and allows access to L1 - S1. This method is a suitable approach for all degenerative disc related indications because it provides immediate access to all of these vertebral levels. However, it is contraindicated in patients with severe spondylolisthesis and significant central canal stenosis due to limited access to the affected area.

2.3.1.6 ALIF

The anterior approach to lumbar interbody fusion is made by creating an anterior mid-line incision which provides some access to the intervertebral disc of the lower lumbar region though it is restricted by vascular anatomy. Therefore, it is only primarily utilized for complete discectomy and spacer implantation at L4/L5 and L5/S1. Additionally, due to the curvature of the spine in the lumbar region, this approach allows for more extensive interbody decompression.[38]

2.3.2 Trends in Lumbar Spine Fusion Procedures

Like any surgical procedure, the lumbar spine fusion field has evolved due to a multitude of factors. A 2019 study by Martin, *et al*. evaluated data from the Agency for Healthcare Research and Quality's National Inpatient Sample between 2004 and 2015 to explore changes in the field with a focus on hospital costs, coding, and demographic data associated with lumbar spine fusions.[5] In 2015, 281,575 lumbar interbody fusion surgeries were performed in the United States, up from 164,527 in 2004.[5] This increase in cases is associated with a rise in procedure-related hospital costs from $8.6 billion to $24.3 billion for all spine

fusions and $3.7 billion to $10.2 billion for just lumbar spine fusions alone. The mean cost per procedure over the 11 year period studied rose from $30,485 to $51,601. The age of patients receiving elective lumbar fusions during this time shifted more heavily towards those at least 65 years old. Surgical interventions used for spondylolisthesis increased the most during this time paralleling increasing patient age. Furthermore, the number of procedures used to treat disc herniation and degeneration, indications with viable non-surgical options, declined from 2010 to 2015. Even with a decline in cases for those indications, the overall volume of lumbar fusions increased during this time period and is expected to continue to increase as the overall population continues to age.

2.4 Materials in Spine Fusion

In order to achieve adequate fusion between vertebral bodies, a graft material is commonly used, often with instrumentation, to create a junction between adjacent vertebrae so to encourage bone growth across the gap resulting in the formation of a solid mineralized bridge.[30,39] An ideal graft material should be the osteoconductive, osteoinductive, and osteogenic (**Table 1**) as these characteristics are inherent to autografts, tissue harvested from elsewhere in the patient.[30,33] In addition to autografts, allografts (*i.e.*, tissue harvested from other patients) and synthetics (*i.e.*, man-made materials) have been commonly utilized to help facilitate spinal fusion.[6,30,40]

Table 1. Terms and definitions of key bone graft material characteristics.

Term	Definition
Osteoconduction	The process where a scaffold allows the ingrowth of host cells, tissue, and vasculature.[41]
Osteoinduction	The process of exogenous factors signal the differentiation of MSCs into osteoblasts.[41]
Osteogenesis	The production of new bone formed solely by osteoprogenitor cells present in the graft.[30]

2.4.1 Autografts

Autografts hold the greatest advantage as graft materials because they are host harvested mineralized tissue that can achieve high quality bone fusion while avoiding undesirable immune response induction.[40] For spine fusion applications, two types of autografts are commonly used: iliac crest bone autograft (ICBG) and local autograft (LAG).[6,7,30] ICBG is harvested from the patient's ileum whereas LAG is the bone removed from the laminae, facets, and/or spinous processes during the decompression process performed at the surgical level(s).[6,30] The supply of LAG is more limited when compared to ICBG, especially when decompression is being carried out at only one level.[7] Despite the limited supply of LAG, mean fusion rates across multiple studies have found it to be slightly higher with it than ICBG (89% versus 79% in one review and 80% versus 76.4% in another).[6,30] This may be due to greater cell proliferation and osteoblast activity in LAG as compared to ICBG when characterized *in vitro*,[42] although this claim has not been directly evaluated *in vivo*. Despite the advantages of autografts, their associated

complications such as donor site morbidity, blood loss, and supply limitations keep them from being a complete solution with no drawbacks.[30]

2.4.2 Allografts

While the two types of autograft material are quite similar, allograft is a broader category when it comes to spine fusion as it includes allogenic bone as well as demineralized bone matrix (DBM).[30,43] Both allografts are generally considered to be osteoconductive, but only DBM retains osteoinductive capabilities, and neither is osteogenic.[30,40] Allogenic bone is cortical or cancellous cadaveric bone that has been frozen or freeze-dried to reduce its antigenicity which unfortunately also removes its osteoinductivity and osteogenic components.[41,43] DBM is processed from cadaveric bone to remove the mineralized phase but retain a network of type 1 collagen and osteoinductive proteins and growth factors.[43] Additionally, DBM is often loaded with manufactured recombinant human bone morphogenic proteins (rhBMPs) to improve its osteoinductive potential. Allogenic bone and DBM are rarely used as standalone grafts, rather, they are most commonly used as autograft extenders in surgery by combining them with either ICBG or LAG.[6,30] In this application, allograft and DBM have fairly substantial fusion results of roughly 80% and 93%, respectively.[30] However, when allogenic bone alone is used in PLLF, the fusion rate is only 52%.[6] Therefore, allogenic bone and DBM are a viable option to be utilized in spine fusion procedures for creating a larger graft volume when combined with autografts, but not when used alone.

2.4.3 Synthetics

Another material type that may be combined with autograft or used alone are synthetic materials.[33] There have been many approaches to creating synthetic bone graft substitutes including formulations comprised of ceramic, polymer, and/or bioactive glass.[33,41,44]

Ceramics used in spine fusion are composed of calcium phosphates (CaP) or calcium silicates and are biocompatible and osteoconductive in nature.[33] They range dramatically in their rate of resorption and delivery mode .[41,45] Generally speaking, calcium sulfate resorbs the quickest (1 - 3 months), followed by tricalcium phosphate (6 - 18 months), and finally hydroxyapatite (HA) is the slowest to resorb (6 months – non-resorbable).[41] The ranges provided are for the broader category of those materials and the particular characteristics depend on the specific form of the ceramic and mode in which it is delivered which includes as a powder, paste, cement, pellets, or pre-formed shapes.[41] Commercial products sometimes utilize a ceramic blend in an attempt to harness the advantages of both types. For example, Medtronic utilizes a biphasic tricalcium phosphate / hydroxyapatite (BCP) blend in their BoneSigma™ BCP product (Medtronic Sofamor Danek, Memphis, TN) and has been reported to have fusion rates ranging from 74.6 - 92.5%.[45]

One common way to locally deliver ceramics is to compound them with a polymeric material. Commercially used polymers for this application include collagen and polymethylmethacrylate (PMMA). Additionally, polymeric materials are rarely used by themselves and mostly employed as graft-extenders with

allograft or autograft. Plantz, *et al.* evaluated in the aggregate 4 studies that assessed either PMMA or a collagen/HA composite (DePuy Synthes Healos, Raynham, MA).[33] Across the studies, Healos was found to underperform ICBG when co-delivered with bone marrow aspirate. Additionally, PMMA demonstrated significantly lower fusion rates when compared to ICBG (0 - 30% versus 86 - 93%, respectively). As a result, PMMA is rarely used for spine fusion. While currently incapable of matching the fusion properties of gold standard approaches, future innovations in polymeric materials may allow for them to be a viable alternative, especially when delivered autologous substances that can incorporate some osteogenic capabilities such as bone marrow aspirate.[33]

Another category of materials used in spine fusion surgeries are bioactive glasses, which have been of particular interest in orthopedic biomaterials as they provide an osteoinductive and osteoconductive substrate for bone growth.[33,41,46] There are many different compositions of bioactive glass that all center on silicon dioxide as their main component. Other minerals that are commonly compounded for their bioactivity and biocompatibility are Na_2O, CaO, P_2O_5, MgO, CaF_2, among others.[33,46] The fusion rate of bioactive glasses vary across studies.[33] When used alone, S53P4 bioactive glass yielded inferior fusion rates compared to autograft alone (71 - 88% and 100%, respectively).[33] When combined with autograft, bioactive glass resulted in no significant difference from autograft alone. Therefore, like other synthetics such as ceramic and polymeric bone graft substitutes, bioactive glass yields its greatest potential when combined with autologous tissue as a bone-graft extender.

2.5 Simple Signaling Tissue Engineering

As the field of biomaterials has advanced, a strong focus has been placed on utilizing the body to heal itself. Tissue engineering scaffolds are aimed at mimicking the body's natural physical, chemical, and biological nature. These are designed around target tissues and cells to encourage them to enhance healing and regeneration. With this in mind, our research group has conducted foundational research on an osteoinductive biomaterial comprised of a dual-crosslinked, cellulose-supported chitosan hydrogel loaded with bioactive CaP.[8-10] The following section will describe the key target and components of this biomaterial as well as provide context for similarly related approaches.

2.5.1 The Target: Mesenchymal Stem Cells

Mesenchymal stem cells (MSCs) have the capacity to differentiate down a number of cell lineages including bone, cartilage, cardiac, hepatic, connective, and adipose, the first of which is the primary interest for spinal fusion applications.[13] MSCs are present in and primarily derived from peripheral blood, bone marrow, adipose, and umbilical cord tissue.[47] Adipose and bone marrow derived MSCs are the most commonly used source for stem cell therapies due to their abundance and ease of harvest – particularly with adipose derived MSCs.[48,49] In the event of tissue damage, local MSCs are able to migrate to defect sites in order to aid in healing making them of significant intertest for tissue engineering and regenerative medicine.[49] These inherent characteristics of MSCs are why they are a primary focus in developing biomaterials.

2.5.2 Endogenous Signaling

Many commercial biomaterials include growth factors and proteins that act as exogenous signals to directly upregulate the osteogenic potential of surrounding cells.[30] This, however, comes with the disadvantage of complex manufacturing and shelf-life considerations, leading to a desire for more simplified materials. A promising alternative is to harness the differentiative power of MSCs through various inducerons, or simple signaling molecules (*i.e.*, SSMs), to achieve the desired cell lineage.[50] Osteoinduction is a key characteristic necessary for regeneration by bone graft materials.[30,33] Osteoblast differentiation has commonly been achieved *in vitro* via supplementing culture media with osteogenic factors such as dexamethasone, β-glycerol phosphate, and ascorbic acid.[14] However, calcium (Ca^{2+}) and phosphate (PO_4^{3-}) ions alone have been shown to be SSMs capable of inducing osteoblast-like activity in MSCs by themselves.[10,51] This was demonstrated by McCullen, *et. al* who showed an increase in mineral deposition with growth media Ca^{2+} levels elevated beyond the physiological concentration of 1.8 mM.[51] Our group's efforts have built upon this seminar work by varying Ca^{2+} and PO_4^{3-} levels to determine a therapeutic window of their osteoinduction.[10] In this work, extracellular Ca^{2+} and PO_4^{3-} concentrations 1 - 16 mM and 1 - 8 mM, respectively, were found to be osteoinductive.[10]

SSMs aim to encourage and upregulate proteinaceous endogenous signaling.[50] Ca^{2+} and PO_4^{3-} ions have been suggested to upregulate bone morphogenic protein-2 (BMP-2), thus providing a basis for their osteoinductive character.[50,52] Interestingly, BMP-2 upregulation does not occur directly through the MSC calcium sensing receptor, but rather through the type L voltage-gated

calcium channel which activates a complex cascade of intracellular signals.[53] Another cell pathway within MSCs that results in osteoblast differentiation is the activation of Wnt.[46] Wnt signaling products stimulate Runx2, a transcription factor protein in osteoblast differentiation. The impact of Ca^{2+} and PO_4^{3-} on Wnt signaling in osteoblast differentiation is not currently well understood. By upregulating cell pathways rather than providing complex exogenous signals, SSMs stimulate a natural healing process driven by the host when delivered with a suitable biomaterial.

2.5.3 Hydrogel Biomaterials

Hydrogels have received considerable attention as candidates for bone tissue engineering materials due to their structural similarities to the extracellular matrix of tissue and their ability to be used to locally deliver osteoinductive factors.[54] A variety of hydrogel biomaterials have also been explored as bone tissue engineering scaffolds including those comprised of collagen, gelatin, hyaluronic acid, fibrin, alginate, elastin, chondroitin, and other synthetics.[54]

Specifically, chitosan has emerged as a biomaterial widely studied for this application.[54-57] This trend may be attributed to an increased understanding of its unique properties and the demand for new

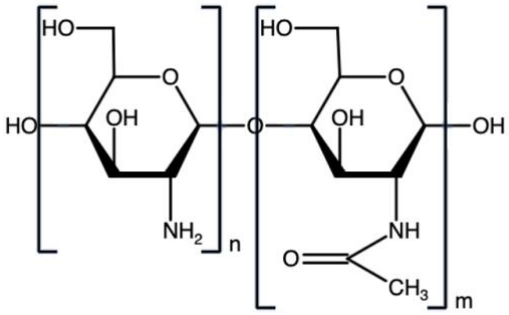

Figure 2. Chemical structure of chitosan. Chitosan consists of acetylated (m) and deacetylated (n) units of D-glucosamine at a ratio based on its degree of deacetylation (*i.e.* DDA).

solutions in the orthopedic biomaterials market.[58,59] Chitosan is a cationic polysaccharide comprised of D-glucosamine and N-acetyl-D-glucosamine subunits (**Figure 2**). It is generated by the chemical processing of chitin (*i.e.*, poly(N-acetyl-D-glucosamine)), a component in the exoskeletons of crustaceans, insects, or fungi.[55] Since chitin is comprised of fully acetylated D-glucosamine subunits, it is hydrophobic and water insoluble making it unsuitable as a hydrogel backbone.[55] However, when chitin is partially deacetylated into chitosan, primary amines are exposed allowing for their protonation conveying some hydrophilicity. Additionally, these amines are highly valuable as a functional group to allow for crosslinking between linear polymer chains to form a semi-solid hydrogel. Chitosan is widely reported to be non-toxic, bioactive, antimicrobial, and biodegradable.[58,60-64] Additionally, through biological degradation mediated by macrophages, the resulting oligomers help signal fibroblasts to synthesize collagen and extracellular matrix.[65] Due to its hydrogel-forming and biodegradation abilities, chitosan allows for the local delivery of drugs, signaling molecules, and other components to improve tissue engineering outcomes.

2.5.4 Osteoinductive Hydrogels

While chitosan hydrogels have many desirable characteristics, they alone do not possess the osteoinductivity and mechanical competency to facilitate bone regeneration for applications like spinal fusion. Therefore, our research group has focused on loading these biomaterials with osteoinductive ceramics and cellulose mechanical reinforcing agents. In our early work, tuning of hydrogels with ionic and covalent bonding crosslinkers allows for control of properties such as ion release,

swelling behavior, and mechanical strength.[8,9] Specifically, it was found that higher ionic and covalent crosslinking ratios to the functional primary amines on chitosan along with the inclusion of cellulose nanocrystals resulted in more-desirable hydrogel mechanical properties.[8] Additionally, PO_4^{3-} was able to be dually-utilized as an ionic crosslinker and a way to effectively deliver this osteoinductive SSM.[8] In our most recent research, the osteoinductive and crosslinking capabilities of PO_4^{3-} were decoupled using dibasic calcium phosphate (*i.e.*, DCP), and carbonate (*i.e.*, CO_3^{2-}), respectively.[9] The aim of this revision was to improve the mechanical properties of the hydrogel as well as provide a donor for the controlled release of both Ca^{2+} and PO_4^{3-} ions. These modifications resulted in improved hydrogel bioactivity, mechanical properties, controlled SSM release, and greater compressive strength.[9]

While there has been much progress made with this material, MSC proliferation was suppressed by ^{0}CNC / C:G:C hydrogels in which the effect of the novel ^{0}CNC cellulose addition will need to be further investigated.

Chapter 3. Materials and Methods

3.1 Formation of Chitosan Hydrogels

3.1.1 Chitosan/Cellulose Solution

To create a chitosan solution, low molecular weight chitosan (m.w. 50,000 - 190,000 Da, Sigma Aldrich) was dissolved in 0.5% acetic acid supplemented deionized, distilled water (ddH_2O) at 1.4% weight/volume and magnetically stirred for 3 days at room temperature followed by gravity filtration through cotton (Fisher Scientific). To mechanically reinforce the chitosan hydrogels, cellulose was chosen as a material. Neutral cellulose nanocrystals (*i.e.*, ^{0}CNCs) were processed from cellulose microcrystals using a previously described method.[8,9] Cellulose nanofibrils (i.e., CNFs) were purchased from the Process Development Center at the University of Maine. CNFs were produced by mechanical grinding wood pulp until fibers approximately 20 – 50 nm in width and several hundred microns in length were produced.[66] ^{0}CNCs or CNFs were added to the chitosan solution at 0.07% weight/volume and dispersed using 10 minutes of sonication via a probe-tip sonicator (Branson Sonifer 450) at 20 W. For osteoinductive ion releasing hydrogels, 6% and/or 10% weight/volume dibasic calcium phosphate (DCP_6, DCP_{10}, Jost Chemical Co.) were added to the chitosan/cellulose solution. The DCP was then dispersed using 1 minute of sonication via the probe-tip sonicator at 20 W.

3.1.2 Crosslinker Solution

A dual crosslinking solution was created by dissolving 42 mg/mL of sodium bicarbonate (*i.e.*, ionic crosslinker) and 28 mg/mL of genipin (*i.e.*, covalent

crosslinker) in ddH_2O followed by 1 minute of sonication via the probe tip sonicator at 20 W. The crosslinking molar ratio was 5:1.25:1 of carbonate : genipin : deacetylated chitosan site (~ 85%). This ratio was chosen based on the advantageous mechanical and bioactive properties previously published with this ratio.[9]

3.1.3 Hydrogel Formation

Hydrogels were formed by adding the appropriate amount of chitosan/cellulose solution to crosslinker solution at a ratio of 5:1 volume/volume followed by 1 second of high-speed mixing on a vortex mixer. The gelation vials were then placed in a 37 °C water bath while they were monitored every 30 seconds for their gelation time. Hydrogels were determined to have gelated upon the material remaining adhered to the bottom of the gelation vials when inverted.[67] After gelation was verified, the hydrogels were allowed to set in a 37 °C incubator for 24 hours before further testing. For allograft-loaded hydrogels, 20% weight/volume crushed cancellous allograft (AG, 0.1 – 4 mm, MTF Biologics) was placed in the gelation vial before the chitosan/cellulose solution and then the crosslinker solution were then added.

3.2 Physical Characterization of Hydrogel

3.2.1 Swelling Ratio

Hydrogel swelling was determined by first submerging preformed hydrogels in phosphate buffered saline (PBS, Gibco) at 37 °C for 24 hours. After 24 hours, the samples were removed from PBS and excess water was removed from the

surface by Kim wipe blotting before they were weighed. The hydrogels were then frozen at - 80 °C and lyophilized under vacuum (0.1 mm Hg) at - 50 °C for 72 hours to ensure all solvent was removed. After lyophilization, the hydrogels were weighed again and swelling ratio was determined using **Equation 1**:

$$\text{Swelling} = \frac{W_w}{W_d} \quad (1)$$

where W_w is the wet hydrogel weight before lyophilization and W_d is the dry hydrogel weight after lyophilization.

3.2.2 Mass Loss

Hydrogel mass loss was measured by submerging the samples in phosphate buffered saline (PBS) at 37 °C. At specific intervals, the samples were removed from solution and excess water was removed from the surface by Kim wipe blotting before they were weighed. After weighing, the hydrogels were gently submerged in the PBS again. Mass loss was calculated using **Equation 2**:

$$\text{Mass Loss } (\%) = \frac{W_0 - W_t}{W_0} \quad (2)$$

where W_0 is the initial weight and W_t is the weight at a specific time point.

3.2.3 Ion Release

Calcium (Ca^{2+}) and phosphate (PO_4^{3-}) ions released from DCP and DCP-loaded hydrogels were measured in ddH_2O at 37°C over 14 days. Preformed hydrogels were immersed in ddH_2O in 24 well plates and DCP powder was placed into 24-well semi-permeable inserts (Greiner Bio-One). At specific timepoints, ddH_2O for each sample was exchanged and assayed for ion content. Ca^{2+} release was evaluated using the Calcium (CPC) LiquiColor™ Test (Stanbio Laboratory). Release samples (1 - 10 µL) were combined with 95 µL of base and color reagent

and mixed. The resultant solution was then read at 550nm using a BioTek Cytation 5 fluorospectrometer. Ca^{2+} ion concentrations were determined by comparing the sample readings to a standard curve (0 - 10 mM). PO_4^{3-} release was measured using a Phosphate Colorimetric Assay (Sigma). Release samples (1 - 100 µL) were combined with 30 µL of assay reagent and diluted with ddH_2O until a final volume of 200 µL was obtained. Solution absorbance was measured at 650 nm and compared to a standard curve (0 - 5 µM) in order to determine the PO_4^{3-} concentration in the samples.

3.2.4 Compressive Strength

Preformed cylindrical hydrogels (height ~ 5 mm and diameter ~ 12 mm) were carefully removed from their gelation vials. Their compressive strength was determined via compression testing using an Instron universal tester. Hydrogels were compressed at a rate of 1 mm/min until 80% strain was achieved at which point the strength was calculated by dividing the maximum force by the compressed hydrogel surface area.

3.3 Assessment of In Vitro Cytotoxicity and Bioactivity

3.3.1 Cell Culture

Murine mesenchymal stem cells (mMSCs) were purchased from Cyagen and stored in the vapor phase of a liquid nitrogen dewar. mMSCs were seeded into T-75 cell culture flasks (CytoOne) and cultured at 37°C in a humidified incubator with 5% CO_2 in complete growth media consisting of Dulbecco's modified Eagle's medium (DMEM, Gibco) supplemented with 10% fetal bovine

serum (FBS, Sigma) and 1% penicillin-streptomycin (Pen-Strep, Gibco). Media was changed every 48 hours until the cells reached ~ 80% confluency at which time they were dissociated using a 0.05% trypsin-EDTA solution (Gibco). Delaminated mMSCs were then counted using a hemocytometer and passed into new T-75 flasks at a splitting ratio of 1:5. Surplus mMSCs were cryopreserved in complete growth media supplemented with 10% DMSO. After the fifth passage, cells were used for *in vitro* studies.

3.3.2 Acute Cytotoxicity

Tissue culture treated 24-well plates (CytoOne) were seeded with 100,000 cells/well and exposed to complete growth media as a negative control. Preformed chitosan hydrogels with no cellulose, ^{0}CNCs, or CNFs (*i.e.* C:G:C 5:1.25:1, ^{0}CNC/C:G:C 5:1.25:1, and CNF/C:G:C 5:1.25:1) were washed twice with PBS and then soaked in 1 mL of complete growth media for 24 hours to create extract media. The extract media was then transferred to the seeded 24 well plates in which the cells were cultured for 24 hours at 37°C in a humidified incubator at 5% CO_2 after which cell quantification and viability assays were conducted on the samples.

3.3.3 Cell Proliferation Assay

Cell proliferation was determined using a Quant-iT™ PicoGreen™ dsDNA Assay (Invitrogen). At each timepoint, cells were washed with PBS and lysed using 1% Triton X-100 (Sigma-Aldrich) followed by three freeze-thaw cycles and sonication via a probe tip sonicator (Branson Sonifer 250) at 10 W to fully lyse the cells. Lysates were diluted with TE buffer (200 mM Tris-HCL, 20 mM EDTA, pH

7.5) and then mixed with PicoGreen reagent according to the manufacturer's recommended protocol. The fluorescence of each sample was read using a BioTek Cytation 5 fluorospectrometer (*ex*. 480 nm, *em*. 520 nm), and cell number was determined using a mMSC standard curve (0 - 250,000 cells/mL).

3.3.4 Cell Viability Assay

Cell viability was evaluated using an alamarBlue™ cell viability reagent (Invitrogen) assay. At each timepoint, all experimental groups were removed from the wells and the cells were gently washed with PBS. The cells were then cultured in complete growth media supplemented with 10% alamarBlue™ reagent for 1 hour at 37 °C in a humidified incubator at 5% CO_2. After incubation, the fluorescence of the alamarBlue™ media for each sample was measured (*ex*. 560 nm, *em*. 590 nm). Cell viability was reported as a ratio of the emission in the experimental groups compared to the group exposed to the complete growth media negative control.

3.3.5 Anti-Abrasion Platform for Inductivity Assessment

A novel anti-abrasion sample platform (**Figure 3**) was developed to remove the impact mechanical stress and diffusion limitations would have if hydrogels were placed directly on top of plated cells. These platforms were printed using an SLA 3D printer (Form 2, Formlabs) and washed using 91% isopropyl alcohol to remove any residual unbound resin. Samples were washed twice with PBS and soaked in complete growth media for 24 hours before being place into wells to support the hydrogel samples during *in vitro* studies. Each group, including non-hydrogel

controls, contained a platform in order to reduce the influence the platform's footprint had on cells.

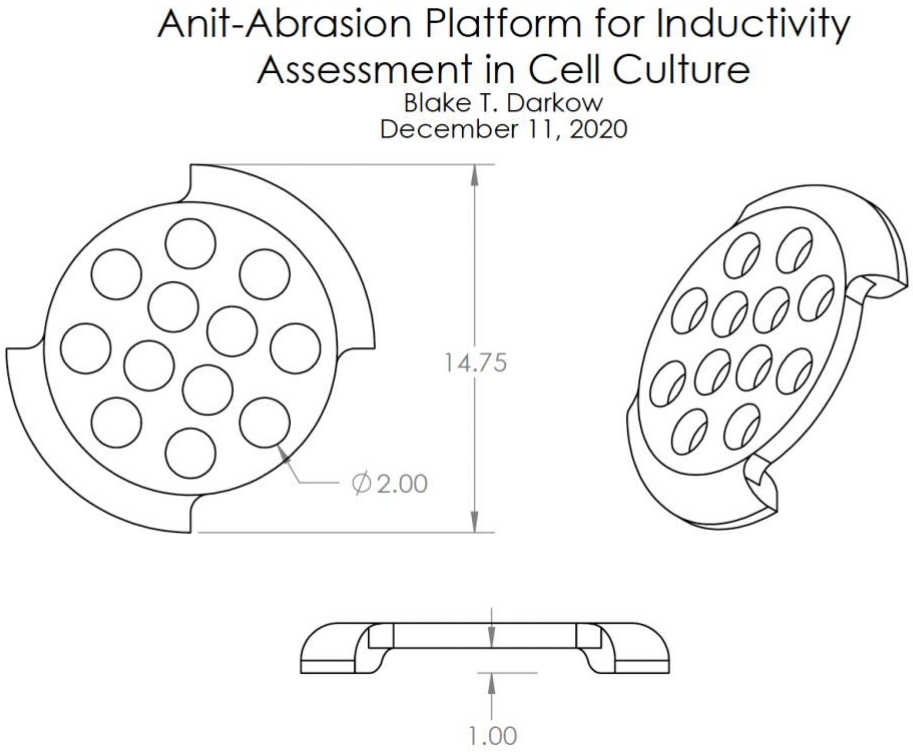

Figure 3. Anti-Abrasion Platform for Inductivity Assessment Cell Culture. The raised platform is perforated to allow mass transfer through and from the biomaterial in question while alleviating the adherent cells from mechanical stress due to contact. Dimensions are in millimeters.

3.3.6 *In Vitro* Bioactivity

Tissue culture treated 24-well plates (CytoOne) were seeded with 50,000 cells/well and exposed to complete growth media as a negative control. Osteogenic media was created by supplementing complete growth media with 2 mM L-glutamine, 50 µM ascorbic acid, 0.1 µM dexamethasone, and 10 mM β-glycerophosphate. CNF/C:G:C 5:1.25:1 hydrogels alone or with DCP_{10} and/or AG

were washed twice with PBS and once with complete growth media. The hydrogels were then gently placed on an in-lab fabricated 3-D printed anti-abrasion platform (Formlabs) in 24-well plates with seeded cells and co-cultured at 37°C in a humidified incubator at 5% CO_2 for which the growth media was changed every two days throughout the study. Cell quantity, viability, alkaline phosphatase activity, and mineralization were evaluated at days 3, 7, 14, and 21.

3.3.7 Alkaline Phosphatase Activity Assay

Cell alkaline phosphatase (i.e., ALP) activity was measured at each time point using an Alkaline Phosphatase Activity kit (BioVision). In brief, 80 µL of cell lysate (harvested as described for the proliferation assay) was combined with 50 µL of 5 mM *p*-nitrophenyl phopshpate (pNPP) in assay buffer. The reaction was incubated for 1 hour at room temperature and then stopped by adding 20 µL of stop solution (NaOH). The absorbance of the resulting solution was read at 405 nm using a BioTek Cytation 5 fluorospectrometer. Absorbance values were converted to enzyme activity by comparing them to a standard curve (0 - 20 µM) of dephosphorylated pNPP (*i.e.*, pNP). ALP activity was reported as pNP content normalized to cell count.

3.3.8 Cell-based Mineralization Assay

Cell-based mineral deposition was measured using an Alizarin Red assay. At each time point, cells were gently washed with ddH_2O and fixed in 70% ethanol for 24 hours. The ethanol was removed and the cells were covered with 1 mL of 40 mM Alizarin Red solution (Sigma-Aldrich) for 10 minutes. The samples were then gently but thoroughly washed with ddH_2O to remove all unbound stain.

Absorbed Alizarin Red stain was then desorbed using a 10% cetylpyridinium chloride (CPC, Sigma-Aldrich) solution which was harvested and its absorbance measured at 550 nm via a BioTek Cytation 5 fluorospectrometer. Absorbance readings were then converted to Alizarin Red concentration using a standard curve (0 - 0.274 mg/mL). The same procedure was performed on acellular 24-well plates that had undergone the same experimental conditions and these values subtracted from the cellularized samples to calculate cell-based mineralization. All values reported were normalized by cell count.

3.4 Statistical Analysis

JMP software was used to make comparisons between experimental groups with Tukey's HSD test specifically employed to determine pairwise statistical differences ($p < 0.05$). Groups that possess different letters have statistically significant differences in mean, whereas those that possess the same letter have means that are statistically insignificant in their differences.

Chapter 4. Results and Discussion

The osteoinductive hydrogel developed in our lab utilizes components that are individually understood to be biocompatible molecules and materials. Even so, the lack of proliferation in MSCs exposed to our hydrogels remains an area requiring further investigation.[8,9] A potential source of MSC suppression is the surface modification of CNCs with cetyltrimethylammonium bromide (CTAB) to produce neutral CNCs (^{0}CNCs). To establish a more biocompatible solution to SSM delivery via a chitosan-based hydrogel, this research explored alternatives to the novel ^{0}CNCs and their impact on the material properties and biocompatibility of the hydrogel.

4.1 Impact of Agent Incorporation on Chitosan Hydrogel Material Properties

Surgical biomaterials that are formed or cured *in situ* require valuable time that must be used judiciously. Therefore, a 20-minute window for a formulation to turn from liquid to gel has been defined.[68] Gelation times for different chitosan hydrogels (*i.e.*, Carbonate:Genipin:Chitosan 5:1.25:1 - C:G:C) varied slightly based on their DCP content and cellulose type (**Figure 4**). The addition of DCP_X (*i.e.*, DCP_6 or DCP_{10}) to the hydrogels resulted in a faster gelation time for DCP_X / C:G:C and CNF / DCP_X / C:G:C hydrogels. The effect of DCP on expediting gelation time may be due to the excess of potential crosslinking agents available because of reversable ionic bonds being formed through the phosphate content of DCP. This finding is consistent with our previously published data.[9] However, DCP incorporation did not yield faster gelation times with either ^{0}CNC / DCP_X / C:G:C hydrogels suggesting that the ^{0}CNCs limit or inhibit DCP mediated-crosslinking.

This effect may be due to the hydrophobicity of ^{0}CNCs reducing the overall generation of additional network crosslinks by DCP. All formulations gelled within the desired 20 minute window making these formulations viable options for time-sensitive *in situ* gelation in a surgical setting.[68]

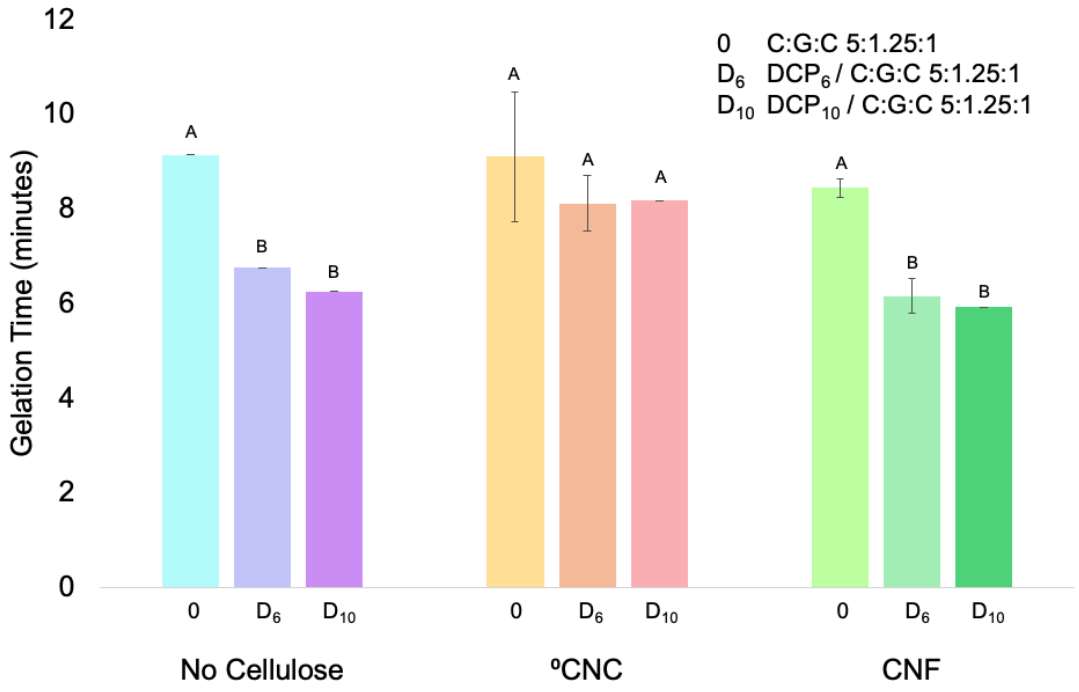

Figure 4. Gelation times for C:G:C 5:1.25:1 hydrogels formed with various cellulose types and DCP concentrations. Hydrogels were prepared with combinations of no cellulose, ^{0}CNCs, or CNFs, without DCP (0), with 6% DCP (D_6), or with 10% DCP (D_{10}). The inversion method at 37 °C was used to determine *in situ* gelation time. Values are reported as the average ± standard deviation (N = 4). Statistical groupings are based on a Tukey's HSD test between all groups. Groups that possess different letters have statistically significant differences ($p < 0.05$) in their means whereas those that possess the same letter are statistically similar.

While gelation time is one important factor for biomaterial utility, its swelling ratio can provide valuable insight into porosity and hydrophilicity. To evaluate the swelling capacity of the hydrogels, the gels were immersed in PBS for 24 hours at 37 °C and then lyophilized. Hydrogel wet weight (pre-lyophilization) and dry weight

(post-lyophilization) were then used to determine the swelling ratio (**Table 2**). The swelling ratio for all hydrogels decreased significantly with the incorporation of DCP. This is likely due to the increase in physical density and crosslinking generated by the inclusion of CaP. The two types of cellulose investigated had different impacts on the swelling ratio compared to the C:G:C hydrogel alone. ^{0}CNC incorporation decreased the swelling ratio across all gel formulations though only statistically significantly for the hydrogels lacking DCP (*i.e.*, C:G:C). A possible explanation for this observation is that the component which gives ^{0}CNCs their neutral surface charge, CTAB, possesses a long alkyl chain (16 hydrocarbons in length) which creates a more hydrophobic environment due to inter- and intra-molecular hydrophobic interactions. Conversely, CNFs increased the swelling ratio for the DCP incorporated hydrogels though only statistically significantly for the DCP_6 group. As the CNFs used in this study are mechanically grinded from wood pulp with no surface modifications,[66] they are relatively hydrophilic in nature,[69] making it unsurprising that CNF incorporation would increase the swellability of the chitosan hydrogel.

Table 2. Swelling ratios for C:G:C 5:1.25:1 hydrogels with various cellulose types and DCP concentrations. This was determined as the wet weight divided by the dry weight after immersion in PBS at 37 °C for 24 hours. Values are reported as the average ± standard deviation (N = 4). Statistical groupings are based on a Tukey's HSD test between all groups. Groups that possess different letters have statistically significant differences ($p < 0.05$) in their means whereas those that possess the same letter are statistically similar.

	C:G:C	DCP_6 / C:G:C	DCP_{10} / C:G:C
No Cellulose	14.55 ± 0.94 (A)	5.76 ± 0.19 (D)	4.73 ± 0.15 (D,E)
^{0}CNC	10.95 ± 0.28 (B)	4.83 ± 0.09 (D,E)	3.94 ± 0.09 (E)
CNF	15.48 ± 0.79 (A)	7.73 ± 0.26 (C)	5.74 ± 0.44 (D)

Another important characteristic of an implantable biomaterial is its ability to retain its components while guiding the body through the healing process. With this in mind, mass loss for the hydrogels was investigated over a one-week period with the day 1, 3, and 7 mass retention ratios presented in **Figure 5**. The largest drop in mass was seen within the first day in which the hydrogels lost 9 - 21% of their mass and the two days after that in which the hydrogels were relieved of another 10 - 20% of their mass. However, beyond day 3, the hydrogels stabilized, like due to the more loosely bound contents having completely dissociated by this time point. When cellulose alone was incorporated into the hydrogels, no differences were observed in mass loss regardless of the formulation. Interestingly, when both cellulose and DCP were incorporated, ^{0}CNCs facilitated statistically significantly greater mass retention at days 3 for both DCP concentrations (*i.e.*, 6 wt. % and 10 wt. %), but only 6 wt. % DCP at day 7. These data are similar to results previously published with ^{0}CNC / DCP_x / C:G:C hydrogels.[9] When DCP begins to dissociate, some PO_4^{3-} ions can remain entrapped in the hydrogel matrix due to their anionic nature facilitating additional ionic crosslinking molecules with open primary chitosan amines available in the network. However, for the hydrogels with no cellulose or with CNFs incorporated, this was not observed. One potential explanation for this result is that, based on the swelling ratio of the respective hydrogels, the no cellulose and CNF hydrogels swell to a much greater extent decreasing their solid mass content and increasing their porosity. This effect limits hydrogel component retention, likely preventing the additional crosslinking

possible with DCP generated PO_4^{3-} and increasing the availability for mass transfer out of the hydrogel as it dissociates.

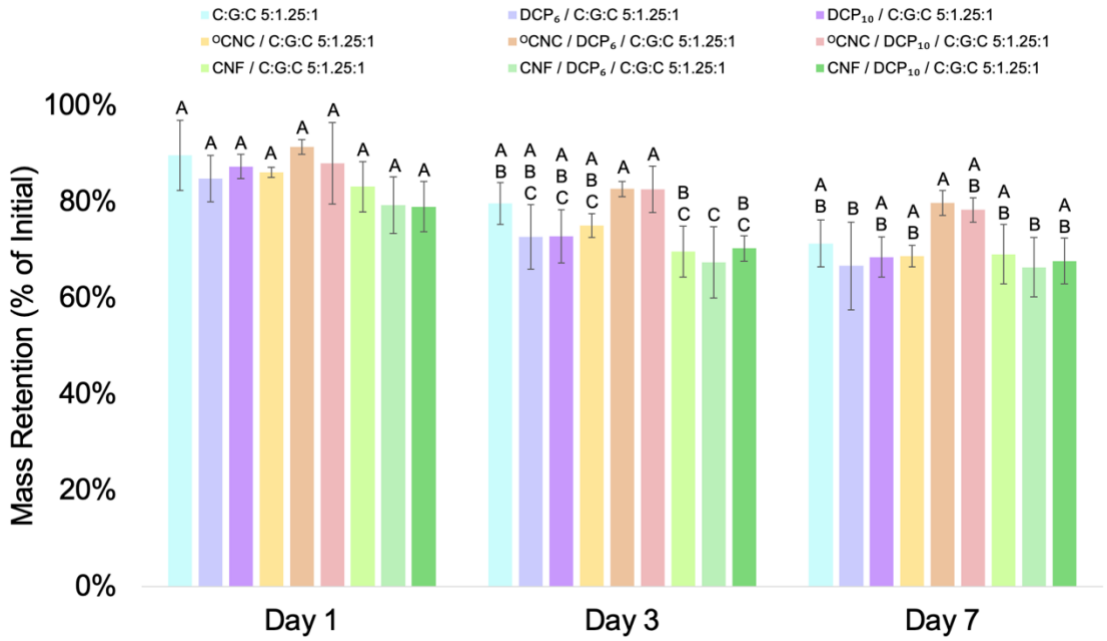

Figure 5. Mass retention for C:G:C 5:1.25:1 hydrogels with various cellulose types and DCP concentrations. This was determined after immersion in PBS at 37 °C for up to 7 days. Values are reported as the average ± standard deviation (N = 4). Statistical groupings are based on a Tukey's HSD test between all groups. Groups that possess different letters have statistically significant differences ($p < 0.05$) in their means whereas those that possess the same letter are statistically similar.

In addition to mass loss by itself being an important factor when considering biomaterial choice, product dissociation also impacts its capacity to facilitate controlled SSM delivery. Release profiles of Ca^{2+} and PO_4^{3-} from DCP and DCP-loaded chitosan hydrogels are presented in **Figure 6**. The overall ion release profile was found to be similar regardless of cellulose type and DCP content. Ca^{2+} release was relatively consistent throughout the 14 days of the experiment (**Figure 6A**). In contrast, hydrogels released the greatest amount of PO_4^{3-} within the first 24 hours (**Figure 6B**). This initial burst of PO_4^{3-} may have been a result of the

hydrogel network having the greatest carbonate-based crosslinking density at the beginning of the study. As evident in the mass loss data, the hydrogel dissociates over time likely freeing up chitosan cationic amines allowing for the negatively charged PO_4^{3-} to remain associated with the positively charged polymer network. This phenomenon also explains why the Ca^{2+} release was much greater than that of the PO_4^{3-}, even though they have equivalent molar ratios within DCP (*i.e.*, chemical formula - $CaHPO_4$). The ion concentrations generated by the dissociation of DCP more or less remains within the previously determined osteoinductive window (*i.e.*, 1 - 16 mM for Ca^{2+} and 1 - 8 mM for PO_4^{3-}) where they are both non-cytotoxic and osteoinductive.[10] In fact, the ion levels never reach the toxic concentrations of 32 mM Ca^{2+} / 16 mM PO_4^{3-} nor the non-bioactive concentrations of 0.5 mM Ca^{2+} / 0.5 mM PO_4^{3-}.[10]

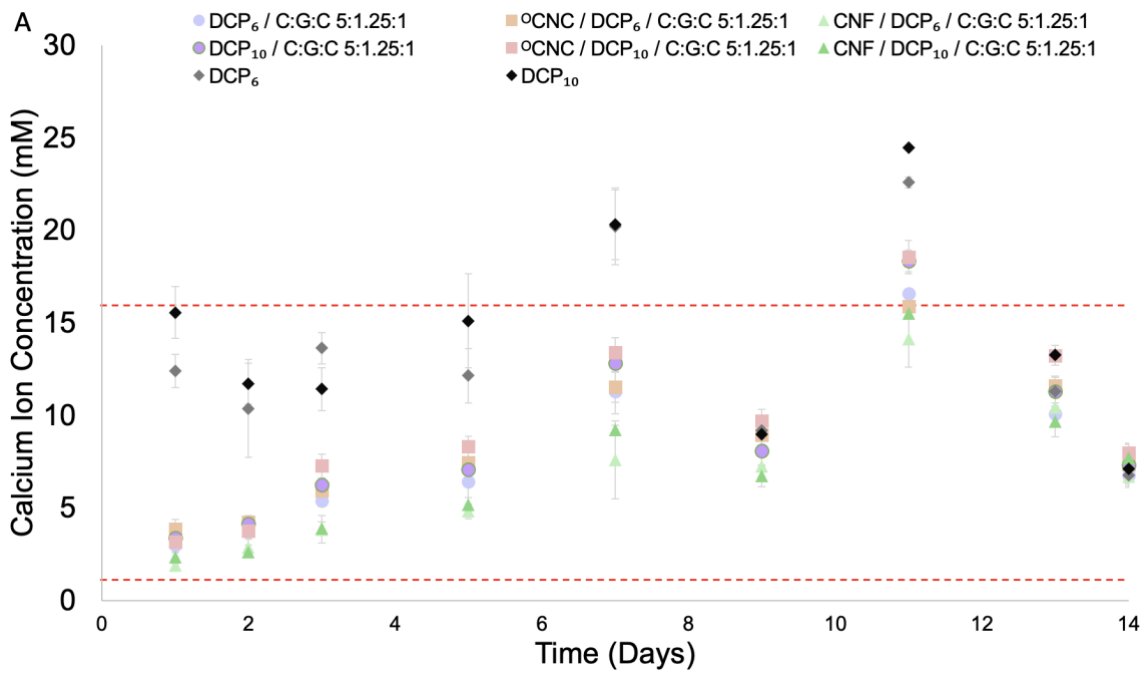

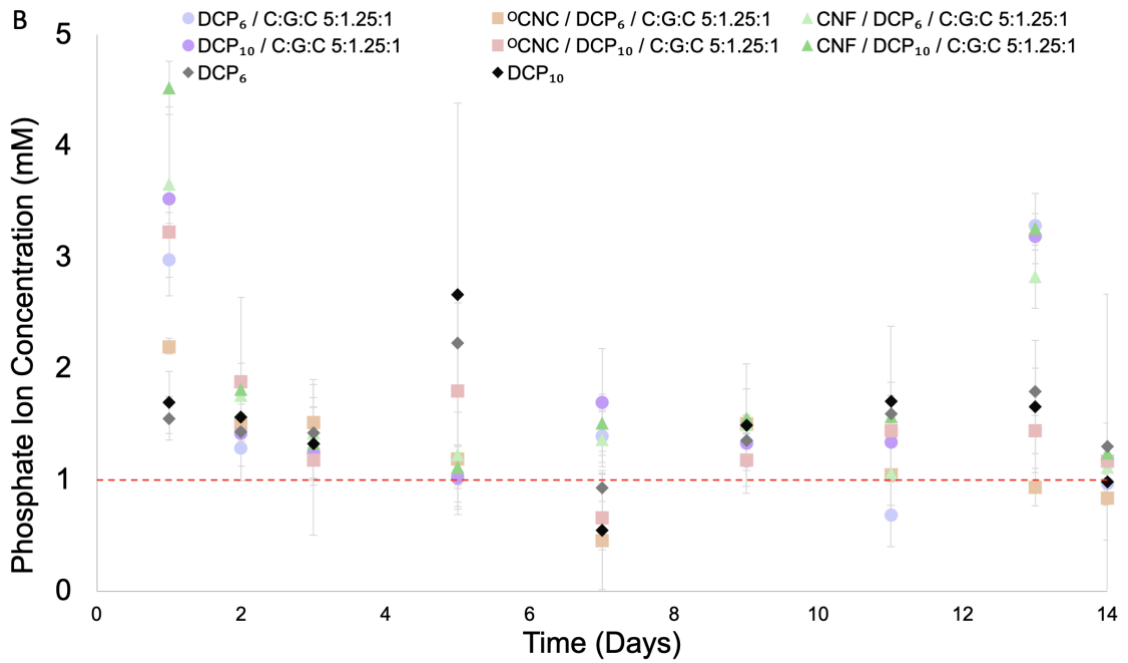

Figure 6. Calcium ion (Ca^{2+}) and phosphate ion (PO_4^{3-}) release concentration from C:G:C 5:1.25:1 hydrogels formed with various cellulose types and DCP concentrations. Hydrogels were prepared with combinations of no cellulose, ^{0}CNCs, or CNFs, without DCP (0), with 6% DCP (D_6), or with 10% DCP (D_{10}). **(A)** Ca^{2+} and **(B)** PO_4^{3-} release from hydrogels immersed in ddH_2O was measured at 37 °C for 14 days. Values are reported as the average ± standard deviation (N = 4). The Ca^{2+} concentration bounds and PO_4^{3-} concentration lower bound of the osteoinductive therapeutic windows are shown with a red line.

While the ion release profile of the implanted material governs its osteoinductivity, the material must also possess the necessary compressive strength to be suitable for weight bearing bone regeneration. The compressive strength of these self-supported hydrogels are displayed in **Figure 7**. The addition of cellulose to the hydrogel without DCP incorporation did result in a slight increase in compressive strength, although this improvement was not statistically significant. Excitingly, the effect of DCP incorporation was highly impactful, especially within the ^{0}CNC and CNF groups. The addition of ceramics like CaP to hydrogels has been widely reported to improve their mechanical strength.[9,70] As

previously discussed, phosphate from DCP can interact with the amine sites on chitosan yielding even greater crosslinking enhancing the mechanics of the material. Independently, ^{0}CNCs and CNFs have also been specifically shown to improve the mechanical strength of hydrogels.[8,71] Nanomaterials have been found to improve the mechanical strength of hydrogels by interlocking neighboring fibers with one another providing additional mechanical support.[71] The synergistic effect observed with DCP and cellulose co-incorporation may be attributable to the overall increased mass density of the hydrogels as well as the cooperative, and not competitive, mechanically reinforcing nature of each component.

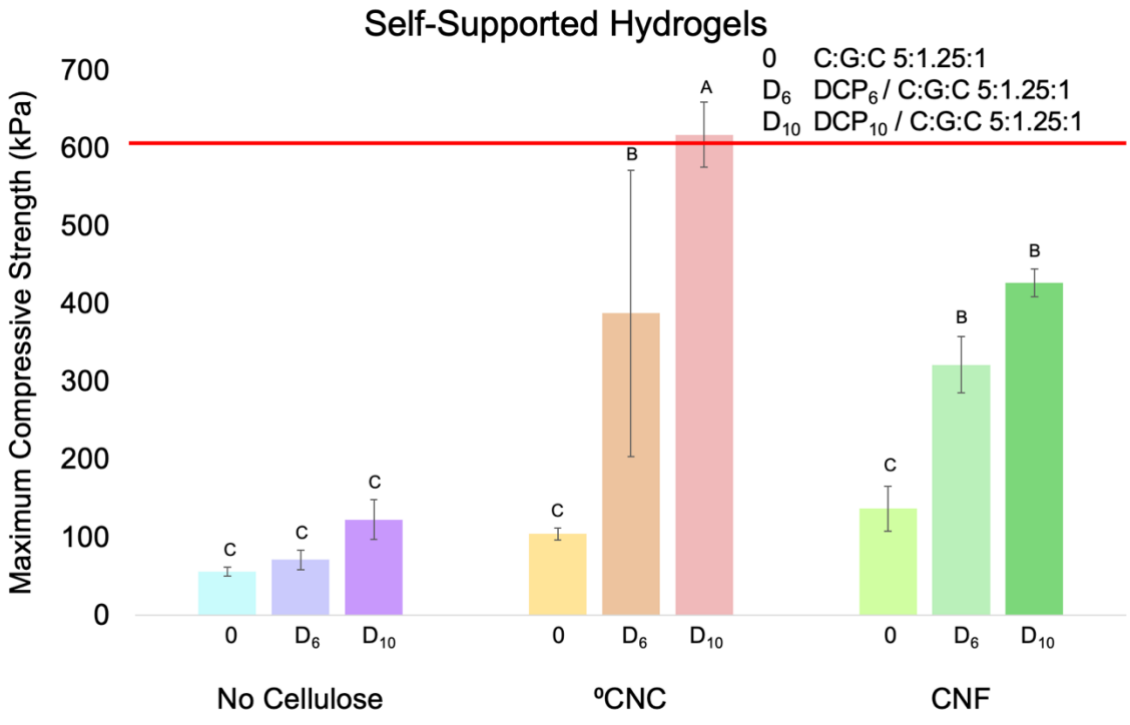

Figure 7. Compression strength for C:G:C 5:1.25:1 hydrogels formed with various cellulose types and DCP concentrations. Hydrogels were prepared with combinations of no cellulose, ^{0}CNCs, or CNFs, without DCP (0), with 6% DCP (D_6), or with 10% DCP (D_{10}). The lower bound of the compressive strength of vertebral bone is indicated with a red line at 600 kPa. Values are reported as the

average ± standard deviation (N = 4). Statistical groupings are based on a Tukey's HSD test performed using all groups shown. Groups that possess different letters have statistically significant differences ($p < 0.05$) in their means whereas those that possess the same letter are statistically similar.

While CNF incorporation improved the compressive strength of C:G:C hydrogels, these formulations still fall below the desired minimum threshold of 600 kPa. A potential way to improve the mechanical strength of hydrogels is to harness the structural integrity of bone itself. To achieve this, chitosan hydrogels were formed around and within crushed cancellous chip allograft (AG). Interestingly, in contrast to the small amount of water exclusion observed during self-supported hydrogel formation, allograft-embedded hydrogels retain the full solution volume used for their synthesis. When tested for their compressive strength, allograft incorporation resulted in a considerable increase in compressive strength (**Figure 8**) when compared to just the inclusion of cellulose and/or DCP into the hydrogel (**Figure 7**). This influence overwhelmed the synergistic impact of cellulose type and/or DCP incorporation into allograft-embedded hydrogels except for the case of the CNF / DCP_6 / C:G:C formulation. In addition to having the highest compressive strength, the CNF / DCP_6 / C:G:C hydrogels tested had remarkedly similar values yielding a very low variance resulting in statistical significance when compared to the CNF / C:G:C hydrogels. Due to the much higher standard deviations calculated with all other allograft-embedded hydrogels, it is much more likely that the CNF / DCP_6 / C:G:C hydrogel samples evaluated did not accurately represent the entire possible sample population rather than a true innate difference existing with this formulation. The improvement in compressive strength measured for allograft-embedded hydrogels provides substantial support for their use as a

biomaterial for bone regeneration applications though their biocompatibility and osteoinductivity still had to be probed *in vitro* before these could ever be assessed *in vivo*.

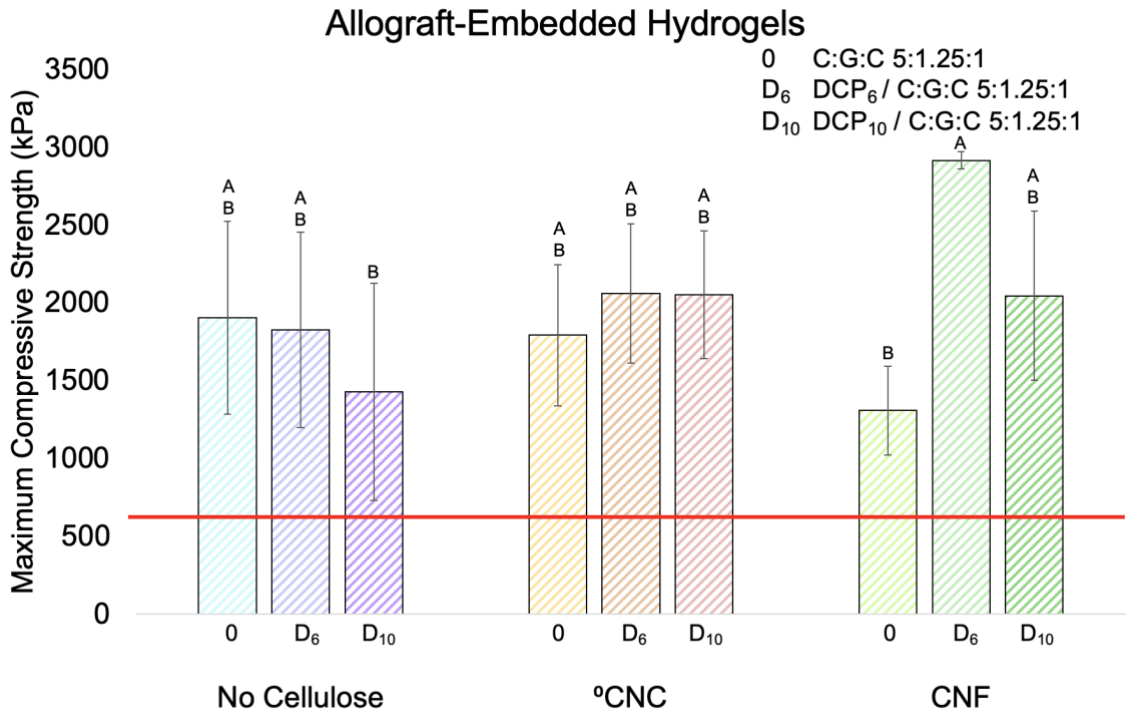

Figure 8. Compression strength for allograft-embedded C:G:C 5:1.25:1 hydrogels with various cellulose types and DCP concentrations. Hydrogels were prepared with combinations of no cellulose, ^{0}CNCs, or CNFs, without DCP (0), with 6% DCP (D_6), or with 10% DCP (D_{10}) all gelated around crushed cancellous chip allograft. The lower bound of the compressive strength of vertebral bone is indicated with a red line at 600 kPa. Values are reported as the average ± standard deviation (N = 4). Statistical groupings are based on a Tukey's HSD test performed using all groups shown. Groups that possess different letters have statistically significant differences ($p < 0.05$) in their means whereas those that possess the same letter are statistically similar.

4.2 Impact of Agent Incorporation on Chitosan Hydrogels Biological Properties

With the effects DCP content, cellulose type, and/or allograft inclusion have on chitosan hydrogel material properties established, their biocompatibility and bioactivity were able to be studied *in vitro* using murine mesenchymal stem cells (mMSCs). To further investigate the potential negative biological side effects observed previously,[8,9] an initial 24-hour cytotoxicity study was performed employing extract media from self-supporting hydrogels prepared with combinations of no cellulose, ^{0}CNCs, or CNFs, without DCP (0), with 6% DCP (D_6), or with 10% DCP (D_{10}). The cytotoxic impact of these biomaterials was determined by comparing the quantity and total metabolic activity of hydrogel extract treated mMSCs using the Quant-iT™ PicoGreen™ dsDNA assay (**Figure 9A**) and an alamarBlue™ assay (**Figure 9B**), respectively, to cells grown in complete growth media alone. Within the no cellulose and CNF hydrogel groups, DCP incorporation had a negative impact on the cells. As this media was transferred to the cells, they would have been exposed to a bolus of the full 24-hour dose of hydrogel dissociated components which could have easily overwhelmed the cells. Interestingly, the ^{0}CNC hydrogels were found to be so cytotoxic that the impact of DCP incorporation could not be effectively studied with these materials. The negative biological impact observed with ^{0}CNC-containing hydrogels is likely attributable to the long alkyl chain associated with the previously mentioned CTAB charge capping group used to generate ^{0}CNCs. This is supported by previous research that found un-bound or detached CTAB can be a potent source of cytotoxicity.[72,73] The incorporation of CNFs into hydrogels facilitated promising

biocompatibility which is unsurprising given the excellent biocompatibility that is inherent to unmodified cellulose.[74,75] This result futher supports CNFs as a promising alternative to ^{0}CNCs. Therefore, ^{0}CNC hydrogels were excluded from further biological testing. Hydrogels with no cellulose as well as the CNF / DCP_6 / C:G:C formulation were also not further tested. While hydrogels with no cellulose possessed promising biocompatibility, they did not exhibit the mechanical properties necessary to be used for vertebral bone regeneration applications (**Figure 7**). Additionally, since CNF / DCP_6 / C:G:C and CNF / DCP_{10} / C:G:C hydrogels had indistinguishable indicators of osteoinductive potential (*i.e.*, SSM release profile and acute biocompatibility), CNF / DCP_{10} / C:G:C hydrogels were chosen because they displayed the potential to be a more mechanically competent formulation (**Figure 7**). Hydrogels with and without AG were also studied due to the considerable enhancement of compressive strength they were able to achieve (**Figure 8**) and the fact that AG is commonly used in spinal fusion procedures.[20,43]

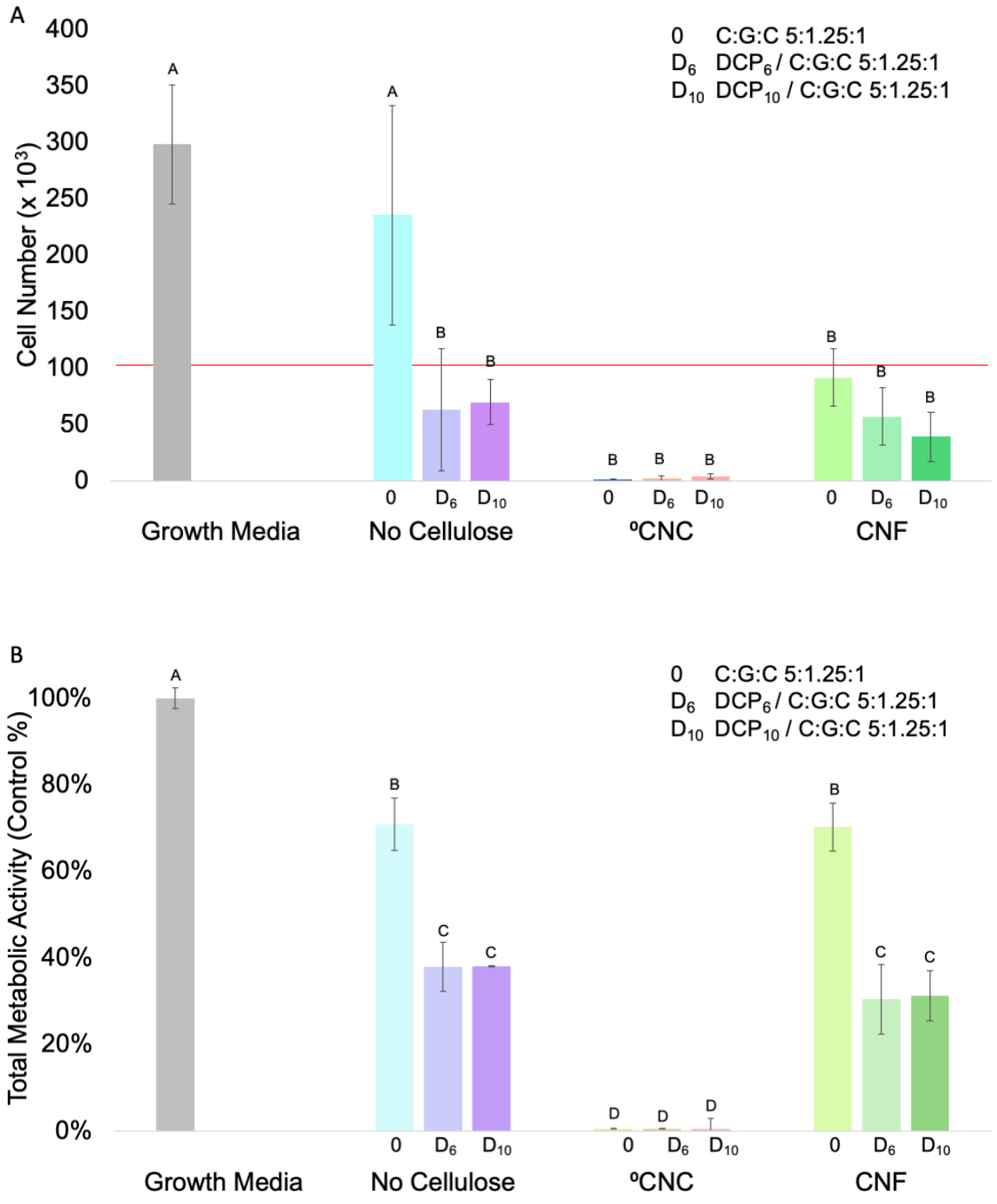

Figure 9. Biocompatibility of self-supported C:G:C 5:1.25:1 hydrogels formed with various cellulose types and DCP concentrations. Hydrogels were prepared with combinations of no cellulose, ^{0}CNCs, or CNFs, without DCP (0), with 6% DCP (D_6), or with 10% DCP (D_{10}). (**A**) Cell proliferation and (**B**) total metabolic activity were measured for cells cultured for 24 hours in extract media at 37°C. As 24-well plates were seeded with 100,000 cells, this is indicated by a red line. Cell number was determined via a Quant-iT™ PicoGreen™ dsDNA assay. Total

metabolic activity was assessed via an alamarBlue™ assay and standardized to control cells cultured in growth media. Data is reported as the mean ± standard deviation (N = 4). Statistical groupings are based on a Tukey's HSD test performed using all groups shown. Groups that possess different letters have statistically significant differences ($p < 0.05$) in means whereas those that possess the same letter are statistically similar.

To evaluate the long-term biocompatibility of the CNF / C:G:C hydrogels, mMSCs were exposed to hydrogels prepared with and without 10% DCP (DCP_{10}) formed with and without AG. Complete growth media and osteogenic media as well as DCP_{10} and allograft delivered via a semi-permeable insert were each used as controls for the hydrogels to evaluate their individual effects on the cells. Biocompatibility was evaluated by measuring the cell proliferation (**Figure 10A**) and total metabolic activity (**Figure 10B**) at 3, 7, 14, and 21 days. DCP_{10} or AG present in semi-permeable inserts had little effect on the quantity and viability of exposed cells at any timepoint compared to growth media. In contrast, cells grown in osteoinductive media lagged in their cell number and viability, suggesting they may have undergone differentiation into osteoblasts.[76] For all hydrogels investigated, exposed cell quantity and viability were significantly lower than all control groups at day 3, indicating some initial toxicity and/or proliferative suppression below the 50,000 starting cell number (*i.e.*, averages of 12,840 - CNF / C:G:C, 10,870 - CNF / DCP_{10} / C:G:C, 43,560 - AG / CNF / C:G:C, and 26,50 - AG / CNF / DCP_{10} / C:G:C). This data parallels the 24-hour cytotoxicity results presented in **Figure 9**. Interestingly, hydrogels with AG (*i.e.*, AG / CNF / C:G:C and AG / CNF / DCP_{10} / C:G:C) less negatively impacted cell numbers than those without AG (*i.e.*, CNF / C:G:C and CNF / DCP_{10} / C:G:C) though incorporating DCP within allograft-embedded hydrogels led to similar suppression seen in **Figure 9**

and made this group have a statistically insignificant difference in its cell count when compared to the self-supported hydrogels. This behavior could be due to highly porous AG acting as a sink and preventing the rapid expulsion of hydrogel components that are believed to have played a role in overwhelming the cells at 24 hours (**Figure 9**). At days 7, 14, and 21, cells exposed to the two hydrogels with AG followed a similar growth pattern as the osteogenic media lagging behind the other three controls (*i.e.*, growth media, DCP_{10}, and AG). Even though the CNF / C:G:C and CNF / DCP_{10} / C:G:C hydrogels suppressed cell growth and viability at day 3, cells exposed to these formulations recovered their quantity and total metabolic activity to those cultured in osteoinductive media by days 7 and 14, respectively. A reason for the later-stage growth is that the hydrogels dissociate rapidly in the first 3 days and stabilizes thereafter (**Figure 5**). Therefore, the cells were likely exposed to a bolus of hydrogel components initially which then slowed after the 3 day window allowing cell populations to recover and grow. The retention of the proliferative capacity of healthy mMSCs when exposed to CNF / C:G:C hydrogels is a promising improvement over our previous °CNC / chitosan hydrogel formulations.[8,9]

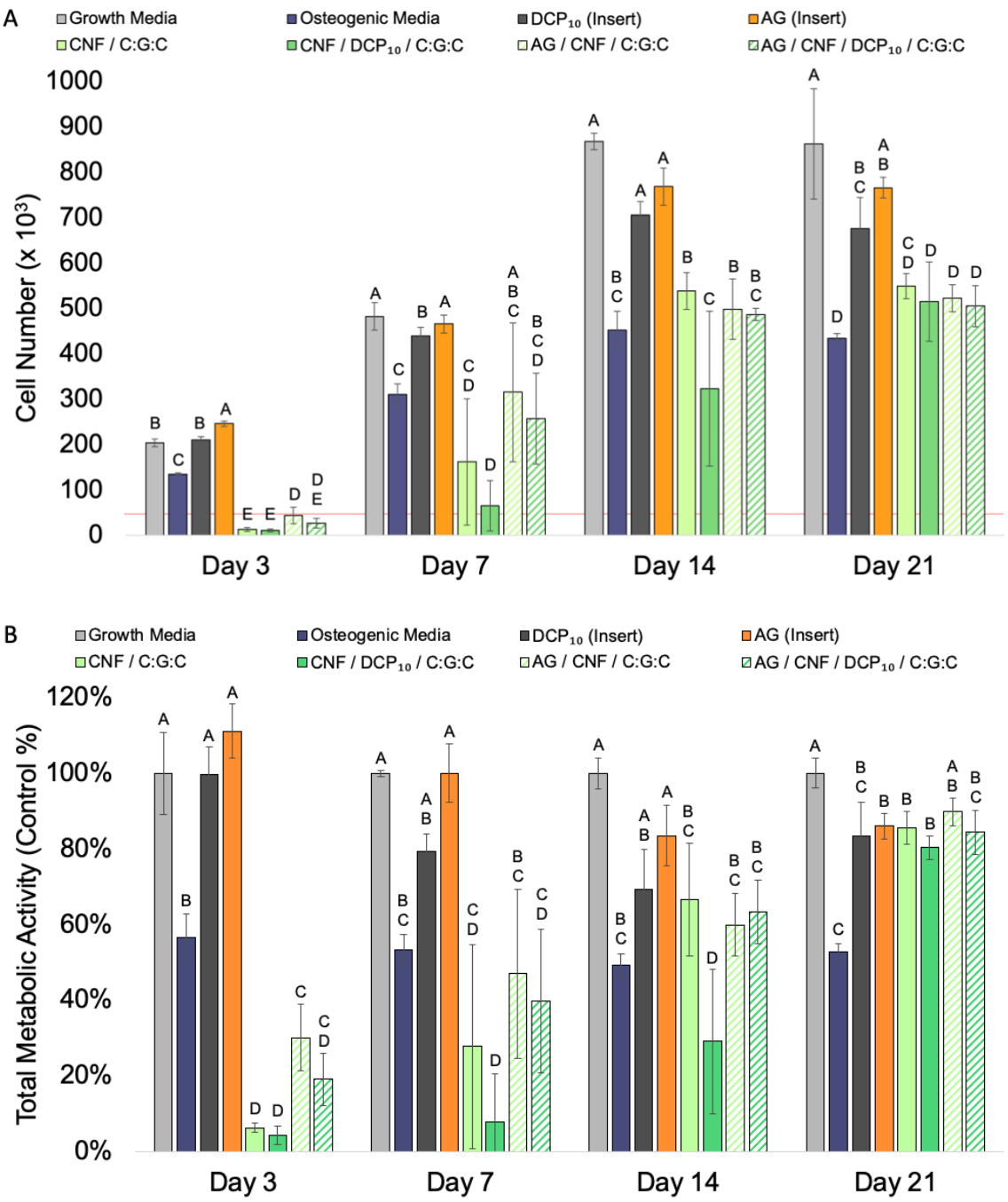

Figure 10. Biocompatibility of self-supported and allograft-embedded CNF / C:G:C hydrogels formed with various DCP concentrations. Hydrogels were prepared with or without DCP_{10} and with or without allograft (AG). (**A**) Cell proliferation and (**B**) metabolic activity were measured for cells cultured for up to 21 days in growth media at 37°C. Cell number was determined via the Quant-iT™ PicoGreen™ dsDNA assay. Total metabolic activity was assessed via an alamarBlue™ assay and standardized to control cells cultured in growth media.

Values are reported as the average ± standard deviation (N = 4). Statistical groupings are based on a Tukey HSD comparison between groups at the same timepoint. Groups that possess different letters have statistically significant differences ($p < 0.05$) in means whereas those that possess the same letter are statistically similar.

To evaluate the osteoinductivity of CNF / C:G:C hydrogels, alkaline phosphatase (ALP) and alizarin red (ALZ) assays were performed on mMSCs cultured with formulations prepared with or without 10% DCP (DCP_{10}) and with or without AG over 21 days (**Figure 11**). Exposing cells to DCP_{10} or AG delivered in semi-permeable inserts had minimal to mild effects on their ALP production whereas those cultured in osteogenic media had statistically significantly higher ALP synthesis at each time point when compared to mMSCs grown in growth media (**Figure 11A**). While a lack of ALP activity when exposed to DCP_{10} seems to contradict our previous results,[8-10] the Ca^{2+} and P_i release concentrations observed in this most recent work differs significantly from our earlier efforts. Specifically, the DCP tested here released high Ca^{2+} and low P_i concentrations near the edges of the therapeutic window likely limiting its inductive capacity. A possible explanation for this discrepancy is the DCP used for this work was from a different batch than the one employed previously though further studies would need to be conducted to explore this effect further. All hydrogel formulations tested induced cells to produce high levels of ALP similar or greater to osteogenic media at day 3. The higher numbers observed with self-supported hydrogels could be related to the very low cell numbers found within those wells (**Figure 10A**). Interestingly, hydrogel-exposed mMSCs saw their ALP production return to baseline levels at the later time points in the study (*i.e.*, days 7, 14, and 21). As

ALP is an early marker of osteoinduction, the results observed for the hydrogel groups may suggest their co-cultured mMSCs are differentiating down an osteogenic lineage.[12]

To complement this early-stage osteoinductivity data, late-stage mineralization as evidenced by CaP ceramic deposition, was studied. This was assessed at the latter two timepoints (*i.e.*, days 14 and 21) via extracellular matrix fixed calcium staining using an Alizarin Red (ALZ) assay (**Figure 11B**). For the groups that showed elevated ALP activity (*i.e.*, osteogenic media and DCP-containing hydrogels), interesting differences in their ALZ results were observed. Osteogenic media did not elevate cell-based mineralization above growth media at either day 14 or day 21. As ALP activity remained elevated through these time points, it is likely that exposure to the osteogenic media was able to initiate osteogenic differentiation, but not facilitate the mMSCs to become full-fledged osteoblasts, a result consistent with previously published research.[42,77] In contrast, though cells exposed to the two DCP-containing hydrogels had background levels of mineralization at day 14, they both had modestly elevated ALZ content significantly greater than mMSCs cultured in growth media. While the overall magnitude of ALZ content on a per cell basis was lower than previously reported,[8,9] the much greater cell numbers seen in this more recent research compensated for this deficiency. Specifically, the analogous hydrogel (*i.e.*, °CNC / DCP_{10} / C:G:C 5:2.5:1) from our published work[9] induced ~ 151 mg of ALZ-stained mineral compared to ~ 119 mg and ~ 172 mg caused by exposure to CNF / DCP_{10} / C:G:C 5:2.5:1 hydrogel and AG / CNF / DCP_{10} / C:G:C 5:2.5:1 hydrogel, respectively. The

combination of early ALP expression and mineralization from cells exposed to DCP-containing hydrogels indicates that these biomaterials are indeed osteoinductive.

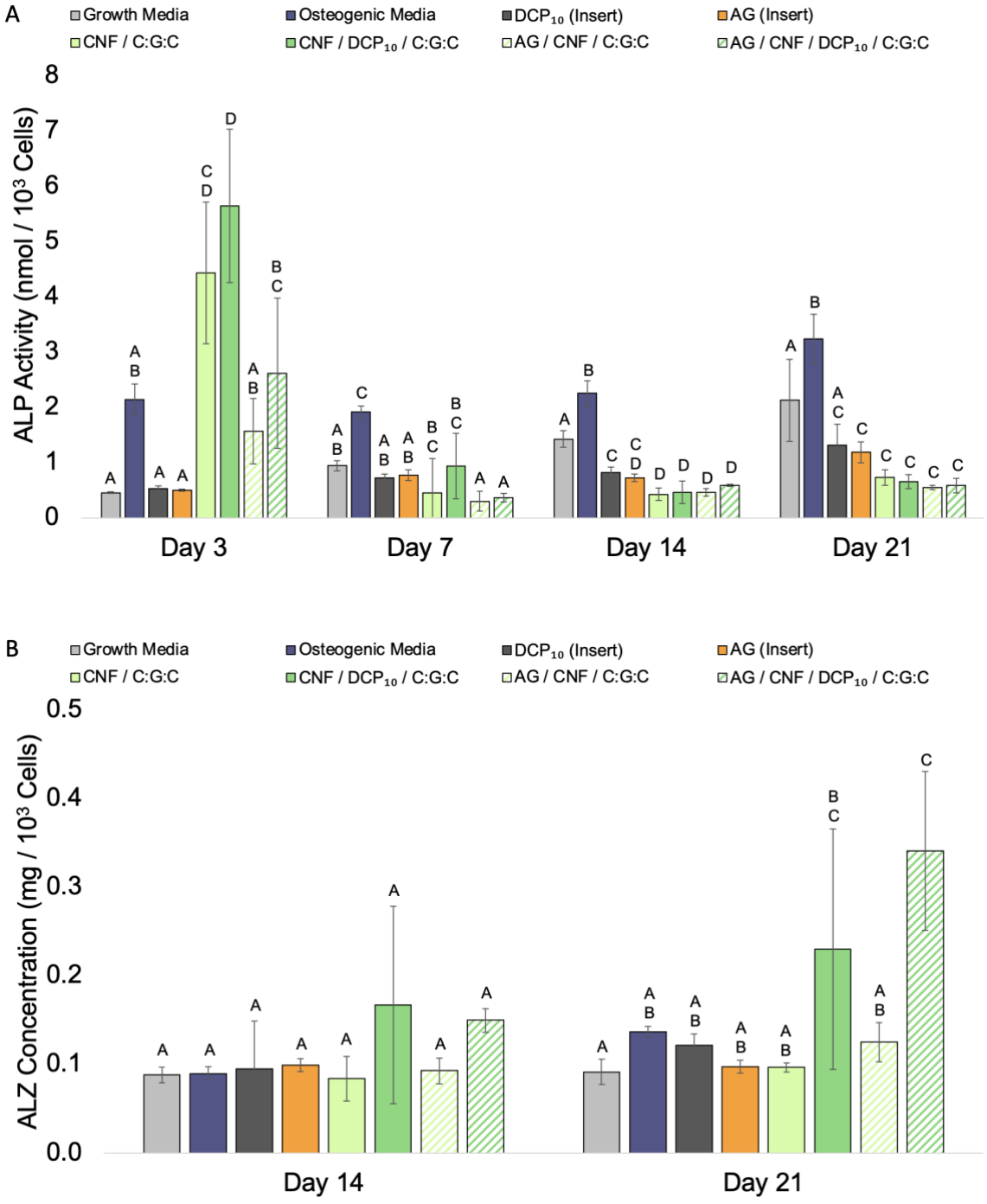

Figure 11. Osteoinductivity of self-supported and allograft-embedded CNF / C:G:C hydrogels formed with various DCP concentrations. Hydrogels were prepared with and without DCP_{10} and with or without allograft (AG). (**A**) ALP activity and (**B**) cell-based mineralization were measured for cells cultured for up to 21 days in growth media at 37°C. ALP activity was determined via an ALP pNPP assay. Alizarin red (ALZ) staining was used as an indirect measure of mineralization with and without hydrogels. ALZ content for matching acellular hydrogel formulations over the same incubation time was subtracted to determine cell-base mineralization. Data is reported as the mean ± standard deviation (N = 4). Statistical groupings are based on a Tukey's HSD test performed using all groups at the same timepoint. Groups that possess different letters have statistically significant differences ($p < 0.05$) in means whereas those that possess the same letter are statistically similar.

Chapter 5. Conclusion and Future Direction

The materials and biological properties determined for the CNF / DCP_{10} / C:G:C and AG / CNF / DCP_{10} / C:G:C hydrogels show tremendous promise for their utility in bone tissue engineering applications. Specifically, these formulations combine desirable gelation time, swellability, resistance to dissociation, ion release, and mechanical strength with biocompatibility and osteoinductivity demonstrating the value of incorporating CNFs, DCP, and AG into chitosan hydrogels. While work previously conducted by our group explored chitosan hydrogels for the controlled release of osteoinductive ions for bone regeneration, significant mMSC proliferation suppression was observed. Before these biomaterials could be translated for clinical applications, they needed to be further modified and optimized. My research has shown that by substituting the mechanically reinforcing agent from cytotoxic ^{0}CNCs to more biocompatible CNFs, hydrogels could be fabricated that possess similar desirable mechanical properties but with improved biological properties. Additionally, AG incorporation into the hydrogels resulted in even greater mechanical strength, biocompatibility, and osteoinductivity when compared to the allograft-free hydrogels. This allograft-embedded hydrogel can serve as a next generation osteoinductive biomaterial especially for weight bearing applications such as in spine fusion procedures.

5.1 *In Vivo* Evaluation of Chitosan Hydrogels

In order to evaluate the performance of bone grafts and bone graft substitutes for spine fusion procedures, a well-validated *in vivo* model utilizing New Zealand White rabbits is frequently employed.[78-82] Before investigating our

hydrogel in this higher order animal model, an *in vivo* biocompatibility study with a lower order animal model should be completed. Additionally, all animal research was conducted with approval of the Animal Care and Use Committee at the University of Missouri - Columbia. Subacute systemic biocompatibility was assessed by implanting a 50 µL hydrogel into the biceps-femoris muscle of C57BL/6 mice followed by close clinical observation. CNF / C:G:C hydrogels were prepared with and without 10% DCP (DCP_{10}) and with or without crushed cancellous chip allograft (AG) (N = 4). Hydrogel groups were compared to 50 µL of normal saline injected into the same site as a control. After 14 days, the mice were humanely euthanized and tissue were collected for histological evaluated to determine the local effects of the formulation on the surrounding tissue. Additionally, the effect of sterile processing of the hydrogels was evaluated. Each hydrogel formulation was subdivided into sterilized or unprocessed subsets. Sterile hydrogels were prepared by combining chitosan and CNFs with and without DCP_{10} and with and without AG that had been autoclaved (30 minutes @ 121 °C) with sterile-filtered crosslinker solution. Unprocessed hydrogels were prepared with all materials not having undergone either sterile process.

During surgical implantation of the hydrogels, 11 mice were lost due to complications with anesthesia. Of the surviving mice, all were found to be healthy through the 14 days of the study. The animals remained bright, alert, and responsive while possessing normal eating and drinking habits and retaining full function of the operated limb. Upon examination of the implant site after euthanasia, all surrounding tissues were evaluated for signs of infection and

inflammation in which no differences were found among the test groups. Harvested tissue was fixed, sectioned, and stained with hematoxylin and eosin (H&E) stain and evaluated for various cell types by a pathologist blinded to the formulation used and physiological responses were recorded in accordance with ISO 10993 – 6. Examination criteria and the results of this study are presented in **Table 3** and **Table 4**, respectively.

Table 3. Examination criteria for histological evaluation of tissue sections. Scoring scale is according to ISO 10993 – 6 "*Biological evaluation of biomedical devices part 6 – test for local effects after implantation*". This table is reprinted from previously published work.[83]

	Score per high power (400X) field (phf)				
Cell type/response	**0**	**1**	**2**	**3**	**4**
Polymorphonuclear cells	0	Rare, 1–5/phf	5–10/phf	Heavy infiltrate	Packed
Lymphocytes	0	Rare, 1–5/phf	5–10/phf	Heavy infiltrate	Packed
Plasma Cells	0	Rare, 1–5/phf	5–10/phf	Heavy infiltrate	Packed
Macrophages	0	Rare, 1–5/phf	5–10/phf	Heavy infiltrate	Packed
Giant cells	0	Rare, 1–5/phf	5–10/phf	Heavy infiltrate	Packed
Necrosis	0	Minimal	Mild	Moderated	Severe
Neovascularization	0	Minimal capillary proliferation, focal, 1–3 buds	Groups of 4–7 capillaries with supporting fibroblastic structures	Broad band of capillaries with supporting structures	Extensive band of capillaries with supporting structures
Fibrosis	0	Narrow band	Moderately thick band	Thick band	Extensive band
Fatty Infiltrate	0	Minimal of fat associated with fibrosis	Several layers of fat and fibrosis	Elongated and broad accumulation of fat cells about the implant site	Extensive fat completely surrounding the implant
Collagen	0	Minimal presence	Mild presence	Moderated presence	Extensive presence
Elastin	0	Minimal presence	Mild presence	Moderated presence	Extensive presence
Traumatic necrosis	0	Minimal	Mild	Moderated	Severe
Foreign debris	0	Minimal	Mild	Moderated	Severe

Table 4. Histology scoring for implanted CNF / C:G:C hydrogels after 14 days. Sterilized (*) and unprocessed CNF / C:G:C hydrogels were prepared with and without 10% DCP (DCP_{10}) and with or without crushed cancellous chip allograft (AG) (N = 4).Values reported as the average score of each group.

	PMN	Lymphocytes	Plasma	Macrophages	Giant	Necrosis	Neovascularization	Fibrosis	Fatty Infiltrate	Traumatic necrosis	Foreign debris	Total
CNF / C:G:C	2	1	0	2	0	0	2	0	0	0	0	7
CNF / C:G:C*	2.6	1.2	0	1.2	0	0	1.4	0	0	0.6	0	7
CNF / DCP_{10} / C:G:C	2.4	1.4	0	1.8	0	0	1.4	0	0	0	0	7
CNF / DCP_{10} / C:G:C*	3	1.6	0	2.2	0.4	0	2.2	0	0	0	0	9.4
AG / CNF / C:G:C	3	1.2	0	1	0	0	2	0	0	0	0	7.2
AG / CNF / C:G:C*	2.25	2	0	1	0	0.25	1.75	0	0	0	0	7.25
AG / CNF / DCP_{10} / C:G:C	2.8	1.2	0	1.2	0	0.6	2.2	0	0	0	0	8
AG / CNF / DCP_{10} / C:G:C*	2.6	1.6	0	1.6	0	0	2	0	0	0	0	7.8

The 14-day biocompatibility study revealed that the chitosan hydrogels tested were non-toxic and therefore cleared for study in higher order animal *in vivo* studies like the rabbit spinal fusion model. Overarching conclusions are difficult to draw from the histological assessment data given that the control was nearly inert to the surrounding tissue and was not able to be evaluated for scoring due to the lack of a physical implant. However, we can still learn about the ongoing physiological processes at day 14 based on the cell populations present in the surrounding tissues. Across all groups, there was a greater presence of polymorphonuclear cells (*i.e.,* PMNs) such as neutrophils which is an early indicator of the foreign body response. There was a slightly lower expression of chronic inflammation markers such as lymphocyte and macrophage infiltration, and no presence of plasma cells. This suggests that the tissue is still in the acute phase of the foreign body response with only modest indications of chronic

inflammation. To allow for stronger conclusions regarding the biocompatibility of the hydrogels to be drawn, an additional group should be studied consisting of the implantation of widely known biocompatible inert material such as polyethylene.

In brief, implant material was placed between the L5/L6 vertebral transverse processes following decortication with a surgical drill. CNF / DCP_{10} / C:G:C and AG / CNF / DCP_{10} / C:G:C hydrogels were compared to the implantation of AG alone. Following 6 weeks, the animals were euthanized and evaluated for fusion via manual palpation. The tissue samples were then fixed in 10% formalin before computed tomography (CT) imaging was performed. Results will be independently analyzed following the conclusion of all trials and collection of histology data from the implant sites though preliminary images from the 6-week time point are shown in **Figure 12**.

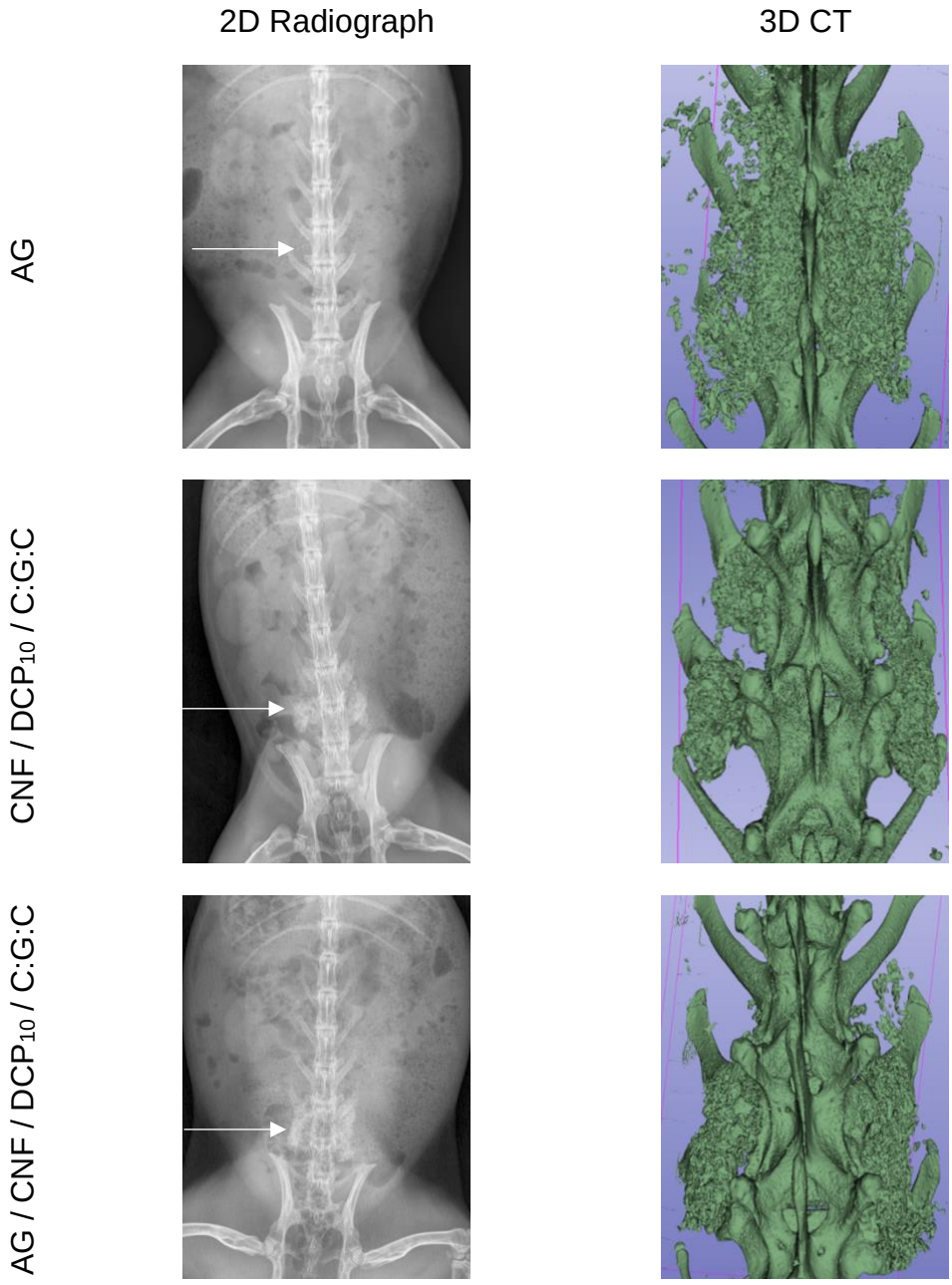

Figure 12. Representative 2D radiographs and rendered CT images of implanted spinal fusion materials at 6 weeks post-operation. Three graft materials (*i.e.*, AG, AG / CNF / DCP_{10} / C:G:C, CNF / DCP_{10} / C:G:C) were evaluated for their ability to achieve fusion in a posterolateral intertransverse process lumbar fusion performed on New Zealand White Rabbits. Implant location is indicated on the 2D radiographs with an arrow. Preliminary data suggests that all groups were able to induce some amount of new mineralized tissue between the vertebral levels.

5.2 Continued Improvement to Chitosan Hydrogels

While there significant improvements to our hydrogel formulation were made through this work, there still exists room for further optimization, particularly on the deliverability of the material. In order to employ hydrogels for spine fusion applications, they can be formed well in advance. However, for other applications that treat spinal disorders, such as vertebral compression fractures (*i.e.*, VCF) addressed by vertebroplasty and/or kyphoplasty, the hydrogel will need to be directly injected.[68] This may be achieved by co-injecting the two solutions simultaneously in order to achieve *in situ* gelation, or given their consistent gelation time (**Figure 4**), the two components may be pre-mixed and injected within the 8 minutes before they fully gelate. This solution is rather straightforward for the hydrogels not containing any AG, but unfortunately is difficult to achieve when AG is to be part of the hydrogel. Specifically, the AG particles are 0.1 - 4.0 mm in size making them too large to pass through a standard injection needle, a potential solution for which is two-fold. First, the AG should be selected down to a smaller diameter that can easily pass through the needle. Second, an injector that utilizes a consistent diameter that the material flows through thereby allowing the contents to easy pass without any dimensional restraints. These improvements would be necessary to conduct planned future *in vivo* studies for VCF repair.

Another area in which this hydrogel should be assessed before it can be translated to the clinic is for its long-term material properties. The ongoing and proposed *in vivo* models last for up to 6 weeks which exceeds any timepoint that has been evaluated *in vitro*. Specifically, dissociation and degradation information

generated from a 6-week mass loss study would be valuable to understand the likely remaining state of the hydrogel at this time point. Degradation, in contrast to dissociation, may be explored by the addition of lysozyme to mimic the enzymatic breakdown of the hydrogel that will occur in the body.[84] Based on these results, further improvements to hydrogel stability can be made by increasing the covalent crosslinking ratios[9] as well as incorporating more stable CaP such as hydroxyapatite (HA).[10] Regardless of the formulation modifications necessary going forward, completion of the current (*i.e.*, rabbit spinal fusion) and future (*i.e.*, rabbit VCF repair) *in vivo* experiments with CNF / DCP_{10} / C:G:C hydrogels will yield important results that will determine the clinical utility of these biomaterials.

References

1. Amin, R.M., Andrade, N.S. & Neuman, B.J. Lumbar Disc Herniation. *Curr Rev Musculoskelet Med* **10**, 507-516 (2017).
2. Andersson, G.B.J. Epidemiological features of chronic low-back pain. *The Lancet* **354**, 581-585 (1999).
3. Baliga, S., Treon, K. & Craig, N.J.A. Low Back Pain: Current Surgical Approaches. *Asian Spine Journal* **9**, 645-657 (2015).
4. Kim, L.H.*, et al.* Expenditures and Health Care Utilization Among Adults With Newly Diagnosed Low Back and Lower Extremity Pain. *JAMA Netw Open* **2**, e193676 (2019).
5. Martin, B.I.*, et al.* Trends in Lumbar Fusion Procedure Rates and Associated Hospital Costs for Degenerative Spinal Diseases in the United States, 2004 to 2015. *Spine (Phila Pa 1976)* **44**, 369-376 (2019).
6. Hsu, W.K.*, et al.* Improving the clinical evidence of bone graft substitute technology in lumbar spine surgery. *Global Spine J* **2**, 239-248 (2012).
7. Mobbs, R.J., Chung, M. & Rao, P.J. Bone graft substitutes for anterior lumbar interbody fusion. *Orthop Surg* **5**, 77-85 (2013).
8. Ghavimi, S.A.A.*, et al.* Inductive co-crosslinking of cellulose nanocrystal/chitosan hydrogels for the treatment of vertebral compression fractures. *Int J Biol Macromol* **130**, 88-98 (2019).
9. Ghavimi, S.A.A.*, et al.* Effect of Dibasic Calcium Phosphate Incorporation on Cellulose Nanocrystal/Chitosan Hydrogel Properties for the Treatment of Vertebral Compression Fractures. *AAPS J* **21**, 1-12 (2019).
10. Ghavimi, S.A.A.*, et al.* Calcium and phosphate ions as simple signaling molecules with versatile osteoinductivity. *Biomed Mater* **13**, 055005 (2018).
11. Crockett, J.C., Rogers, M.J., Coxon, F.P., Hocking, L.J. & Helfrich, M.H. Bone remodelling at a glance. *J Cell Sci* **124**, 991-998 (2011).
12. Rutkovskiy, A., Stenslokken, K.O. & Vaage, I.J. Osteoblast Differentiation at a Glance. *Med Sci Monit Basic Res* **22**, 95-106 (2016).
13. Pittenger, M.F.*, et al.* Mesenchymal stem cell perspective: cell biology to clinical progress. *NPJ Regen Med* **4**, 22 (2019).
14. Pittenger, M.F., Mackay, A.M. & Marshak, D.R. Multilineage potential of adult human mesenchymal stem cells. *Science* **284**, 143-147 (1999).
15. Long, F. Building strong bones: molecular regulation of the osteoblast lineage. *Nat Rev Mol Cell Biol* **13**, 27-38 (2012).
16. Metzger, C.E. & Narayanan, S.A. The Role of Osteocytes in Inflammatory Bone Loss. *Front Endocrinol (Lausanne)* **10**, 285 (2019).
17. M. Zaidi, A.M.I., B.S Moonga, P.J.R. Bevis, C.L.-H. Huang. Forty years of calcitonin—where are we now? A tribute to the work of Iain Macintyre, FRS. *Bone* **30**, 655-663 (2002).
18. Khosla, S., Oursler, M.J. & Monroe, D.G. Estrogen and the skeleton. *Trends Endocrinol Metab* **23**, 576-581 (2012).

19. B. Lawrence Riggs, S.K., L. Joseph Melton. A Unitary Model for Involutional Osteoporosis: EstrogenDeficiency Causes Both Type I and Type II Osteoporosisin Postmenopausal Women and Contributes to Bone Lossin Aging Men. *Journal of Bone and Mineral Research* **13**, 763-773 (1998).
20. Frost, B.A., Camarero-Espinosa, S. & Foster, E.J. Materials for the Spine: Anatomy, Problems, and Solutions. *Materials (Basel)* **12**(2019).
21. Harris, I.A., Traeger, A., Stanford, R., Maher, C.G. & Buchbinder, R. Lumbar spine fusion: what is the evidence? *Intern Med J* **48**, 1430-1434 (2018).
22. Teraguchi, M.*, et al.* Prevalence and distribution of intervertebral disc degeneration over the entire spine in a population-based cohort: the Wakayama Spine Study. *Osteoarthritis Cartilage* **22**, 104-110 (2014).
23. Kos, N., Gradisnik, L. & Velnar, T. A Brief Review of the Degenerative Intervertebral Disc Disease. *Med Arch* **73**, 421-424 (2019).
24. Arts, M.P.*, et al.* Comparison of treatments for lumbar disc herniation: Systematic review with network meta-analysis. *Medicine (Baltimore)* **98**, e14410 (2019).
25. Frymoyer, J.W. Back Pain and Sciatica. *New Egnland Journal of Medicine* **318**, 291-300 (1988).
26. Gagnet, P., Kern, K., Andrews, K., Elgafy, H. & Ebraheim, N. Spondylolysis and spondylolisthesis: A review of the literature. *J Orthop* **15**, 404-407 (2018).
27. Fredrickson, B.E., Baker, D., McHolick, W.J., Yuan, H.A. & Lubicky, J.P. The natural history of spondylolysis and spondylolisthesis. *The Journal of Bone & Joint Surgery* **66**, 699-707 (1984).
28. Bagley, C.*, et al.* Current concepts and recent advances in understanding and managing lumbar spine stenosis. *F1000Res* **8**(2019).
29. Ishimoto, Y.*, et al.* Associations between radiographic lumbar spinal stenosis and clinical symptoms in the general population: the Wakayama Spine Study. *Osteoarthritis Cartilage* **21**, 783-788 (2013).
30. Morris, M.T., Tarpada, S.P. & Cho, W. Bone graft materials for posterolateral fusion made simple: a systematic review. *Eur Spine J* **27**, 1856-1867 (2018).
31. Mobbs, R.J., Phan, K., Malham, G., Seex, K. & Rao, P.J. Lumbar interbody fusion: techniques, indications and comparison of interbody fusion options including PLIF, TLIF, MI-TLIF, OLIF/ATP, LLIF and ALIF. *J Spine Surg* **1**, 2-18 (2015).
32. Chatham, L.S., Patel, V.V., Yakacki, C.M. & Dana Carpenter, R. Interbody Spacer Material Properties and Design Conformity for Reducing Subsidence During Lumbar Interbody Fusion. *J Biomech Eng* **139**(2017).
33. Plantz, M.A., Gerlach, E.B. & Hsu, W.K. Synthetic Bone Graft Materials in Spine Fusion: Current Evidence and Future Trends. *Int J Spine Surg* **15**, 104-112 (2021).
34. Virk, S., Qureshi, S. & Sandhu, H. History of Spinal Fusion: Where We Came from and Where We Are Going. *HSS J* **16**, 137-142 (2020).
35. Lestini, W.F., Fulghum, J.S. & Whitehurst, L.A. Lumbar spinal fusion: advantages of posterior lumbar interbody fusion. *Surg Technol Int* **3**, 577-590 (1994).
36. Malham, G.M., Parker, R.M., Goss, B. & Blecher, C.M. Clinical results and limitations of indirect decompression in spinal stenosis with laterally implanted

interbody cages: results from a prospective cohort study. *Eur Spine J* **24 Suppl 3**, 339-345 (2015).
37. Malham, G.M. & Ellis, N. Maintenance of Segmental Lordosis and Disc Height in Standalone and Instrumented Extreme Lateral Interbody Fusion (XLIF). *Clin Spine Surg* **30**(2017).
38. Bateman, D.K.*, et al.* Anterior lumbar spine surgery: a systematic review and meta-analysis of associated complications. *Spine J* **15**, 1118-1132 (2015).
39. Katchko, K., Schneider, A.D. & Hsu, W.K. Lumbar Interbody Fusion Implant Materials. *Comtemporary Spine Surgery* **18**, 1-8 (2017).
40. Fillingham, Y. & Jacobs, J. Bone grafts and their substitues. *The Bone & Joint Journal* **98**, 6-9 (2016).
41. Roberts, T.T. & Rosenbaum, A.J. Bone grafts, bone substitutes and orthobiologics: the bridge between basic science and clinical advancements in fracture healing. *Organogenesis* **8**, 114-124 (2012).
42. Defino, H.L.A.*, et al.* In Vitro Proliferation and Osteoblastic Phenotype Expression of Cells Derived From Human Vertebral Lamina and Iliac Crest. *Spine* **34**, 1549-1553 (2009).
43. Cohen, J.D., Kanim, L.E., Tronits, A.J. & Bae, H.W. Allografts and Spinal Fusion. *Int J Spine Surg* **15**, 68-93 (2021).
44. Bohner, M., Galea, L. & Doebelin, N. Calcium phosphate bone graft substitutes: Failures and hopes. *Journal of the European Ceramic Society* **32**, 2663-2671 (2012).
45. Nickoli, M.S. & Hsu, W.K. Ceramic-based bone grafts as a bone grafts extender for lumbar spine arthrodesis: a systematic review. *Global Spine J* **4**, 211-216 (2014).
46. Fiani, B., Jarrah, R., Shields, J. & Sekhon, M. Enhanced biomaterials: systematic review of alternatives to supplement spine fusion including silicon nitride, bioactive glass, amino peptide bone graft, and tantalum. *Neurosurg Focus* **50**, E10 (2021).
47. Oryan, A., Kamali, A., Moshiri, A. & Baghaban Eslaminejad, M. Role of Mesenchymal Stem Cells in Bone Regenerative Medicine: What Is the Evidence? *Cells Tissues Organs* **204**, 59-83 (2017).
48. Nordberg, R.C. & Loboa, E.G. Our Fat Future: Translating Adipose Stem Cell Therapy. *Stem Cells Transl Med* **4**, 974-979 (2015).
49. Murphy, M.B., Moncivais, K. & Caplan, A.I. Mesenchymal stem cells: environmentally responsive therapeutics for regenerative medicine. *Exp Mol Med* **45**, e54 (2013).
50. Cushnie, E.K.*, et al.* Simple signaling molecules for inductive bone regenerative engineering. *PLoS One* **9**, e101627 (2014).
51. McCullen, S.D., Zhan, J., Onorato, M.L., Bernacki, S.H. & Loboa, E.G. Effect of Varied Ionic Calcium on Human Adipose-Derived Stem Cell Mineralization. *Tissue Eng* **16**, 1971-1981 (2010).

52. Chai, Y.C., Roberts, S.J., Schrooten, J. & Luyten, F.P. Probing the osteoinductive effect of calcium phosphate by using an in vitro biomimetic model. *Tissue Eng Part A* **17**, 1083-1097 (2011).
53. Barradas, A.M.*, et al.* A calcium-induced signaling cascade leading to osteogenic differentiation of human bone marrow-derived mesenchymal stromal cells. *Biomaterials* **33**, 3205-3215 (2012).
54. Liu, M.*, et al.* Injectable hydrogels for cartilage and bone tissue engineering. *Bone Res* **5**, 17014 (2017).
55. Deepthi, S., Venkatesan, J., Kim, S.K., Bumgardner, J.D. & Jayakumar, R. An overview of chitin or chitosan/nano ceramic composite scaffolds for bone tissue engineering. *Int J Biol Macromol* **93**, 1338-1353 (2016).
56. Muzzarelli, R.A., El Mehtedi, M., Bottegoni, C., Aquili, A. & Gigante, A. Genipin-Crosslinked Chitosan Gels and Scaffolds for Tissue Engineering and Regeneration of Cartilage and Bone. *Mar Drugs* **13**, 7314-7338 (2015).
57. Kjalarsdottir, L.*, et al.* Bone remodeling effect of a chitosan and calcium phosphate-based composite. *Regen Biomater* **6**, 241-247 (2019).
58. Rodriguez-Vazquez, M., Vega-Ruiz, B., Ramos-Zuniga, R., Saldana-Koppel, D.A. & Quinones-Olvera, L.F. Chitosan and Its Potential Use as a Scaffold for Tissue Engineering in Regenerative Medicine. *Biomed Res Int* **2015**, 1-15 (2015).
59. Stewart, S.K. Fracture Non-Union: A Review of Clinical Challenges and Future Research Needs. *Malays Orthop J* **13**, 1-10 (2019).
60. Lewandowska-Lancucka, J.*, et al.* Genipin crosslinked bioactive collagen/chitosan/hyaluronic acid injectable hydrogels structurally amended via covalent attachment of surface-modified silica particles. *Int J Biol Macromol* **136**, 1196-1208 (2019).
61. Dimida, S.*, et al.* Genipin-cross-linked chitosan-based hydrogels: Reaction kinetics and structure-related characteristics. *Journal of Applied Polymer Science* **132**, 42256 (2015).
62. Dhivya, S., Saravanan, S., Sastry, T.P. & Selvamurugan, N. Nanohydroxyapatite-reinforced chitosan composite hydrogel for bone tissue repair in vitro and in vivo. *J Nanobiotechnology* **13**, 1-13 (2015).
63. Suo, H.*, et al.* Interpenetrating polymer network hydrogels composed of chitosan and photocrosslinkable gelatin with enhanced mechanical properties for tissue engineering. *Mater Sci Eng C Mater Biol Appl* **92**, 612-620 (2018).
64. Owczarz, P., Rył, A., Dziubiński, M. & Sielski, J. Injectable Chitosan Scaffolds with Calcium β-Glycerophosphate as the Only Neutralizing Agent. *Processes* **7**, 1-18 (2019).
65. Vaca-Cornejo, F., Reyes, H.M., Jimenez, S.H.D., Velazquez, R.A.L. & Jimenez, J.M.D. Pilot Study Using a Chitosan-Hydroxyapatite Implant for Guided Alveolar Bone Growth in Patients with Chronic Periodontitis. *J Funct Biomater* **8**(2017).
66. Maine, T.U.o. Nanocellulose Data Sheets. (2022).
67. Nair, L.S., Starnes, T. & Ko, J.-W.K. Development of Injectable Thermogelling Chitosan–Inorganic Phosphate Solutions for Biomedical Applications. *Biomacromolecules* **8**, 3779-3785 (2007).

68. Moglia, R.S*., et al.* Injectable polymerized high internal phase emulsions with rapid in situ curing. *Biomacromolecules* **15**, 2870-2878 (2014).
69. Chami Khazraji, A. & Robert, S. Interaction Effects between Cellulose and Water in Nanocrystalline and Amorphous Regions: A Novel Approach Using Molecular Modeling. *Journal of Nanomaterials* **2013**, 1-10 (2013).
70. Islam, M.M., Shahruzzaman, M., Biswas, S., Nurus Sakib, M. & Rashid, T.U. Chitosan based bioactive materials in tissue engineering applications-A review. *Bioact Mater* **5**, 164-183 (2020).
71. Abe, K. & Yano, H. Cellulose nanofiber-based hydrogels with high mechanical strength. *Cellulose* **19**, 1907-1912 (2012).
72. Alkilany, A.M*., et al.* Cellular uptake and cytotoxicity of gold nanorods: molecular origin of cytotoxicity and surface effects. *Small* **5**, 701-708 (2009).
73. Ricles, L.M., Nam, S.Y., Trevino, E.A., Emelianov, S.Y. & Suggs, L.J. A Dual Gold Nanoparticle System for Mesenchymal Stem Cell Tracking. *J Mater Chem B* **2**, 8220-8230 (2014).
74. Ana Gouveia, M.M., et al. . Preparation, Characterization and In Vivo Biocompatibility Studies of Cotton Cellulose Nanofibers. *J. Nanosci. Nanotechnol* **20**, 6532-6541 (2020).
75. Hickey, R.J. & Pelling, A.E. Cellulose Biomaterials for Tissue Engineering. *Front Bioeng Biotechnol* **7**, 45 (2019).
76. Glueck, M*., et al.* Induction of Osteogenic Differentiation in Human Mesenchymal Stem Cells by Crosstalk with Osteoblasts. *Biores Open Access* **4**, 121-130 (2015).
77. Ressler, A*., et al.* Injectable chitosan-hydroxyapatite hydrogels promote the osteogenic differentiation of mesenchymal stem cells. *Carbohydr Polym* **197**, 469-477 (2018).
78. Ghodasra, J.H., Daley, E.L., Hsu, E.L. & Hsu, W.K. Factors influencing arthrodesis rates in a rabbit posterolateral spine model with iliac crest autograft. *Eur Spine J* **23**, 426-434 (2014).
79. Riordan, A.M., Rangarajan, R., Balts, J.W., Hsu, W.K. & Anderson, P.A. Reliability of the rabbit postero-lateral spinal fusion model: A meta-analysis. *J Orthop Res* **31**, 1261-1269 (2013).
80. Palumbo, M., Valdes, M., Robertson, A., Sheikh, S. & Lucas, P. Posterolateral intertransverse lumbar arthrodesis in the New Zealand White rabbit model: I. Surgical anatomy. *Spine J* **4**, 287-292 (2004).
81. Valdes, M., Palumbo, M., Appel, A.J., McAllister, S. & Ehrlich, M. Posterolateral intertransverse lumbar arthrodesis in the New Zealand White rabbit model: II. Operative technique. *Spine J* **4**, 293-299 (2004).
82. Virk, S.S., Coble, D., Bertone, A.L., Hussein, H.H. & Khan, S.N. Experimental Design and Surgical Approach to Create a Spinal Fusion Model in a New Zealand White Rabbit (Oryctolagus cuniculus). *J Invest Surg* **30**, 226-234 (2017).
83. Osorio, M*., et al.* Ex Vivo and In Vivo Biocompatibility Assessment (Blood and Tissue) of Three-Dimensional Bacterial Nanocellulose Biomaterials for Soft Tissue Implants. *Sci Rep* **9**, 10553 (2019).

84. Ganji, F., Abdekhodaie, M.J. & Ramazani S.A, A. Gelation time and degradation rate of chitosan-based injectable hydrogel. *Journal of Sol-Gel Science and Technology* **42**, 47-53 (2007).